UNIVERSITY OF CALIFORNIA, SAN DIEGO

Studies of transport and thermalization of excitons and the development of techniques for *in-situ* manipulation of excitons in coupled quantum wells

A dissertation submitted in partial satisfaction of the
requirements for the degree
Doctor of Philosophy

in

Physics

by

Aaron Tynes Hammack

Committee in charge:

Professor Leonid V. Butov, Chair
Professor Dmitri N. Basov
Professor Michael M. Fogler
Professor Yeshaiahu Fainman
Professor Charles W. Tu

2010

The dissertation of Aaron Tynes Hammack is approved, and it is acceptable in quality and form for publication on microfilm and electronically:

_____

_____

_____

_____

_____
Chair

University of California, San Diego

2010

DEDICATION

To Tamara, light of my life, and to my wonderfully supportive and loving family.

TABLE OF CONTENTS

LIST OF FIGURES

LIST OF TABLES

ACKNOWLEDGEMENTS

I would like to start with a sincere thanks to my advisor, Professor Leonid Butov, for his support of my research and for his wonderful tutelage. His adherence to the highest scientific standards and profound knowledge of the physics of excitons has been an inspiration throughout the pursuit of my Ph.D. His passion for physics is exceeded only by the care that he has taken to insure that his students have an enjoyable and productive environment in which to grow their own love for physics. He is always available for discussion and guidance and has fostered an environment where we are driven in our experiments by the beauty of the natural world and the camaraderie with our colleagues.

A large debt of gratitude also goes to our theory collaborators at the University of Cardiff, lead by Professor Alex Ivanov. The models presented within this dissertation are the result of an incredibly fruitful collaboration between our two laboratories. In specific, Lois Smallwood, Leonidas Mouchliadis, Joe Wilkes, and Egor Muljarov were immensely helpful in the development of the model for exciton transport and thermalization and the simulations demonstrating the strong concordance with measurements.

Nikolai Gippius also deserves a special thanks for his work in developing the general purpose electrostatic simulator that enabled us to open the exciting field of laterally tunable potential reliefs for excitons with reduced exciton dissociation.

Professor Arthur Gossard and those who have worked with him throughout the years, especially Micah Hanson and Ken Campman, deserve a special thanks for their expertise in growth of III-V quantum wells that has made our studies of indirect excitons possible.

I would like to thank Professor Michael Fogler for his general assistance on exciton theory, and for his help in linking our optical interference measurements to the underlying exciton physics. I would also like to thank Sen Yang for all of his helpful discussions, and for a wonderful six years together in the lab. Speaking with Sen over the years broadened my horizons, his acumen with theoretical physics and his love of history and world politics leading to many

engaging and enriching discussions. I would also like to thank Alex High for his beautiful work in the further development of excitonic devices and a for a wonderful friendship both in and outside of the lab.

Jason Leonard and Alex Winbow deserve specific thanks for their numerous engaging discussions regarding theory (Jason) and the intricate details of experimental implementation (Alex). I would also like to thank Mikas Remeika, Gabriele Grosso, Joe Graves, Yuliya Kuznetsova, Erik Shipton, Greg Andreev, Martin Griswold, Erik Green, and James Lohner for all of their help in experiments, discussions, and simulations.

I thank my parents and my grandparents for their wonderful support and guidance throughout my life. It is to them that I owe my passion for knowledge and my love of learning.

Finally, I want to thank Tamara for standing with me as a beautiful companion and for brightening my days during our many years together.

The text of chapter 4, in part, is a reprint of the material as it appears in AL Ivanov, LE Smallwood, AT Hammack, Sen Yang, LV Butov, & AC Gossard, *Origin of the inner ring in photoluminescence patterns of quantum well excitons*, Europhys Lett, **73**, 920 © 2006 European Physical Society, where the dissertation author was the first experimental author. The co-authors in this publication directed, supervised, and co-worked on the research with forms the basis of this chapter.

The text of chapter 4, in part, is a reprint of the material as it appears in AT Hammack, LV Butov, J Wilkes, L Mouchliadis, EA Muljarov, AL Ivanov, & AC Gossard, *Kinetics of the inner ring in the exciton emission pattern in coupled GaAs quantum wells*, Phys Rev B **80**, 155331, © 2007 The American Physical Society, where the dissertation author was the first author. The co-authors in this publication directed, supervised, and co-worked on the research with forms the basis of this chapter.

The text of chapter 5, in part, is a reprint of the material as it appears in AT Hammack, M Griswold, LV Butov, LE Smallwood, AL Ivanov, & AC Gossard,

Trapping of cold excitons in quantum well structures with laser light, Phys Rev Lett **96**, 227402, © 2006 The American Physical Society, where the dissertation author was the first author. The co-authors in this publication directed, supervised, and co-worked on the research with forms the basis of this chapter.

The text of chapter 5, in part, is a reprint of the material as it appears in AT Hammack, LV Butov, L Mouchliadis, AL Ivanov, & AC Gossard, *Kinetics of indirect excitons in an optically induced trap in GaAs quantum wells*, Phys Rev B **76**, 193308, © 2009 The American Institute of Physics, where the dissertation author was the first author. The co-authors in this publication directed, supervised, and co-worked on the research with forms the basis of this chapter.

The text of chapter 6, in part, is a reprint of the material as it appears in AT Hammack, NA Gippius, Sen Yang, GO Andreev, LV Butov, M Hanson, & AC Gossard, *Excitons in electrostatic traps*, J Appl Phys **99**, 066104, © 2006 The American Physical Society, where the dissertation author was the first author. The co-authors in this publication directed, supervised, and co-worked on the research with forms the basis of this chapter.

VITA

2001	Bachelor of Science in Electrical Engineering and Computer Science, University of California, Berkeley
2002-2003	Research Assistant, Department of Physics, University of California, Berkeley
2003-2005	Graduate Teaching Assistant, Department of Physics, University of California, San Diego
2003-2010	Graduate Research Assistant, Department of Physics, University of California, San Diego
2010	Doctor of Philosophy in Physics, University of California, San Diego

PUBLICATIONS

Hammack AT, Butov LV, Wilkes J, Mouchliadis L, Muljarov EA, Ivanov AL, & Gossard AC. *Kinetics of the inner ring in the exciton emission pattern in coupled GaAs quantum wells*. Phys Rev B, **80**(15), 155331 [2009].

Grosso G, Graves JC, Hammack AT, High AA, Butov LV, Hanson M, & Gossard AC. *Excitonic switches operating at around 100 K*. Nat Photonics, **3**(10), 577 [2009].

High AA, Thomas AK, Grosso G, Remeika M, Hammack AT, Meyertholen AD, Fogler MM, Butov LV, Hanson M, & Gossard AC. *Trapping indirect excitons in a GaAs quantum-well structure with a diamond-shaped electrostatic trap*. Phys Rev Lett, **103**(8), 087403 [2009b].

High AA, Hammack AT, Butov LV, Mouchliadis L, Ivanov AL, Hanson M, & Gossard AC. *Indirect excitons in elevated traps*. Nano Lett, **9**(5), 2094 [2009a].

Remeika M, Graves JC, Hammack AT, Meyertholen AD, Fogler MM, Butov LV, Hanson M, & Gossard AC. *Localization-delocalization transition of indirect excitons in lateral electrostatic lattices*. Phys Rev Lett, **102**(18), 186803 [2009].

Fogler MM, Yang S, Hammack AT, Butov LV, & Gossard AC. *Effect of spatial resolution on the estimates of the coherence length of excitons in quantum wells*. Phys Rev B, **78**(3), 035411 [2008].

Hammack AT, Butov LV, Mouchliadis L, Ivanov AL, & Gossard AC. *Kinetics of indirect excitons in an optically induced trap in GaAs quantum wells*. Phys Rev B, **76**(19), 193308 [2007].

High AA, Hammack AT, Butov LV, Hanson M, & Gossard AC. *Exciton optoelectronic transistor*. Opt Lett, **32**(17), 2466 [2007].

Winbow AG, Hammack AT, Butov LV, & Gossard AC. *Photon storage with nanosecond switching in coupled quantum well nanostructures*. Nano Lett, **7**(5), 1349 [2007].

Yang S, Mintsev AV, Hammack AT, Butov LV, & Gossard AC. *Repulsive interaction in the macroscopically ordered exciton state in GaAs/Al_xGa_{1-x}As coupled quantum well structures*. Phys Rev B, **75**(3), 033311 [2007].

Yang S, Hammack AT, Fogler MM, Butov LV, & Gossard AC. *Coherence length of cold exciton gases in coupled quantum wells*. Phys Rev Lett, **97**(18), 187402 [2006].

Hammack AT, Griswold M, Butov LV, Smallwood LE, Ivanov AL, & Gossard AC. *Trapping of cold excitons in quantum well structures with laser light*. Phys Rev Lett, **96**(22), 227402 [2006b].

Hammack AT, Gippius NA, Yang S, Andreev GO, Butov LV, Hanson M, & Gossard AC. *Excitons in electrostatic traps*. J Appl Phys, **99**(6), 066104 [2006a].

Ivanov AL, Smallwood LE, Hammack AT, Yang S, Butov LV, & Gossard AC. *Origin of the inner ring in photoluminescence patterns of quantum well excitons*. Europhys Lett, **73**(6), 920 [2006].

Nagaoka K, Comstock MJ, Hammack A, & Crommie MF. *Observation of spatially inhomogeneous electronic structure of Si(100) using scanning tunneling spectroscopy*. Phys Rev B, **71**(12), 121304(R) [2005].

ABSTRACT OF THE DISSERTATION

Studies of transport and thermalization of excitons and the development of techniques for *in-situ* manipulation of excitons in coupled quantum wells

by

Aaron Tynes Hammack

Doctor of Philosophy in Physics

University of California, San Diego, 2010

Professor Leonid V. Butov, Chair

The study of excitons in semiconductors is a rich field that has seen numerous beautiful developments during the seven decades since they were proposed by Frenkel [1931]. The exciton states in dielectric materials and molecular complexes are fundamental to understanding the full electronic structure of materials and the complex interactions between light and matter. Of particular interest is the fact that excitons, bound electron-hole pairs, form composite bosons with very low effective masses. This opens up an incredibly rich opportunity to study the phase space of quantum degenerate Bose gases at relatively high temperatures. An overview of many of the rich features that have been observed in exciton gases is presented. The system of indirect excitons in coupled quantum wells (CQWs) provides for drastically increased and tunable exciton lifetimes, leading to improved thermalization. The present experimental study presents a full steady state and dynamic model for the transport, generation, recombination, and thermalization of indirect excitons in CQWs, as well as methods for *in-situ* manipulation of indirect excitons by both optical and electrical methods.

Both the optical and electrical methods for exciton control provide for dynamic manipulation of excitons on timescales significantly shorter than the lifetimes of indirect excitons.

1 Introduction

1.1 Motivation

An exciton is a bound pair of an electron and a hole in a semiconductor. More than 40 years ago Keldysh & Kozlov [1968] demonstrated that in the dilute limit, excitons are weakly interacting hydrogen-like bosons. Similarly to electrons or holes, excitons flow within the semiconductor lattice, however, their bosonic character and neutral charge changes the transport dynamics in fundamental ways. One of the more exciting differences is that excitons are expected to undergo Bose-Einstein condensation (BEC) at relatively high temperatures. The degeneracy temperature of a gas of quantum mechanical particles scales inversely with the mass of the particles. In the system of excitons, the mass M_X is small, and BEC should occur at temperatures on the order of 1 K for readily accessible densities. These temperatures are orders of magnitude higher than those required for atomic gases and results in an excellent model system to investigate fundamental quantum mechanical behavior for macroscopic ensembles of bosons

The classical and quantum degenerate character of exciton transport, resulting photo-luminescent pattern formation, and techniques for the manipulation of exciton flow in coupled quantum wells (CQWs) are the focal topics of the research presented within this dissertation.

1.2 Outline of the dissertation

In chapter 2, we briefly review the properties of excitons in both bulk semiconductors and in QWs. The specific benefits of indirect excitons in GaAs/AlGaAs CQWs, which are the focus of the studies in this dissertation, are introduced.

In chapter 3, we briefly review the experimental techniques used for these studies. An overview of the sample structure is also provided.

In chapter 4, an overview of exciton transport and in-depth steady-state and kinetic models of the emergence and evolution of the inner ring photoluminescent pattern observed in the emission from spot excitation of GaAs CQWs are presented.

In chapter 5, a novel optical method for *in-situ* control of exciton density, temperature, and transport is presented along with the application of the general steady-state and kinetic transport models from chapter 4 to explain the behaviors that are observed.

In chapter 6, an electrostatic model is presented for *in-situ* control of excitons. Laterally modulated electrodes enable virtually arbitrary energy landscapes for indirect excitons in CQWs, while careful positioning of the CQWs within the sample minimizes the field induced dissociation of the excitons. Experimental proof of principle for the implementation of traps formed by patterned electrodes on a sample geometry calculated from the model is presented along with an overview of the devices for electrostatic control of exciton flow that have since been developed.

In chapter 7, a brief summary of the current work is presented along with a brief introduction to current investigations and future studies.

2 Excitons

2.1 Introduction to excitons

An exciton is a quasiparticle found in semiconductors, insulators, and molecular complexes that consists of a negatively charged electron bound to a positively charged hole. It is an elementary excitation of condensed matter that was first proposed by Yakov Frenkel in 1931 [Frenkel, 1931], when he described the collective excitation of the atoms in an insulating crystal lattice. Frenkel proposed that such an excited state could travel through the lattice without the net transfer of charge.

Excitons resulting from photo-excitation of semiconductors or photo-excitation of molecular complexes are the type most frequently studied though it is possible for excitons to form whenever electrons and holes interact within a material. When a photon enters a material with sufficient energy, it can excite an electron from the valence band into the conduction band for semiconductors or insulators, or from the highest occupied molecular orbital (HOMO) to the lowest unoccupied molecular orbital (LUMO) in molecular complexes. This photo excitation of the electrons leaves a hole of opposite electric charge, to which the electron is bound by the Coulomb force. As a result, in many semiconducting, or insulating, material systems, such as bulk or nano-structured GaAs, the exciton is at lower energy than the unbound electron and hole, and thus forms a ground state for the excited electrons and holes.

Depending on the properties of the material in which they are embedded, excitons are treated by two limiting cases: (i) Frenkel excitons, where the Coulomb interaction of the electron and hole is relatively unscreened by the

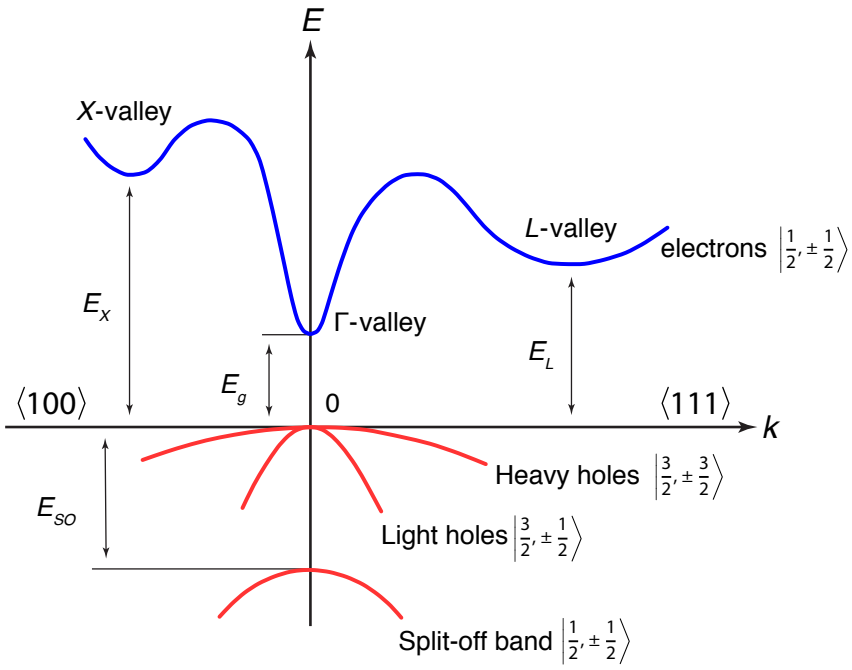

Figure 2.1: Bulk GaAs band structure. The conduction band is shown in blue, while the valence bands, consisting of the heavy hole (HH), light hole (LH), and split-off (SO) bands are shown in red.

material and (ii) Wannier-Mott excitons [Wannier, 1937], where the Coulomb interaction between the electrons and holes is screened strongly by a high polarization of the material. Frenkel excitons tend to be small and strongly bound, while Wannier-Mott excitons are large and weakly bound. Given the large dielectric constant of most semiconductors and insulators, Wannier-Mott excitons are the type most frequently ecountered in semiconductor optics, and are the focus of this dissertation.

2.2 Exciton spin

One of the key features of excitons that gives rise to their interesting quantum mechanical properties at low temperature is that they are composite bosons. Bosons are particles possessing integral spin, given that excitons are

formed from an electron and a hole, both fermions possessing half integral spin, the total intrinsic angular momentum for the exciton will be an integer. However, the specific character of the spin states for electrons and holes within a given material is in itself a rather broad topic, so for the sake of brevity we focus on the spin states of carriers in GaAs, which is the material primarily investigated in this dissertation. The basic principles are similar for most semiconductor materials.

Figure 2.1 shows the band structure of bulk GaAs. In GaAs the conduction band electron is in an s-orbital like state, with $l_e = 0$ and $s_e = \frac{1}{2}$ thereby having a total angular quantum number of $j_e = l_e + s_e = \frac{1}{2}$ and corresponding states of $|j_e, m_e\rangle \in \left|\frac{1}{2}, \frac{1}{2}\right\rangle, \left|\frac{1}{2}, -\frac{1}{2}\right\rangle$. In contrast, the wave-function for the holes, which reside in the valence band, resembles a p-orbital state, with the associated quantum numbers, $l_h \in 0, 1$ and $s_h = \frac{1}{2}$, leading to a total angular quantum number of $j_h = l_h + s_h$, so that $j_h \in \{\frac{1}{2}, \frac{3}{2}\}$.

The energy difference between the different j_h states are mainly due to spin orbit interaction, which is governed by the hamiltonian

$$\mathcal{H}_{\text{so}} = \gamma_{\text{so}} \boldsymbol{L} \cdot \boldsymbol{S} \tag{2.1}$$

where γ_{so} is a constant determined by the material parameters. Using the definition $\boldsymbol{J} \equiv \boldsymbol{L} + \boldsymbol{S}$ we can derive that

$$\boldsymbol{J}^2 = (\boldsymbol{L} + \boldsymbol{S})^2 \tag{2.2}$$

$$= \boldsymbol{L}^2 + \boldsymbol{S}^2 + 2\boldsymbol{L} \cdot \boldsymbol{S}. \tag{2.3}$$

and hence that the interaction energy is

$$E_{\text{so}} = \gamma_{\text{so}} \langle \mathcal{H}_{\text{so}} \rangle \tag{2.4}$$

$$= \frac{\gamma \hbar^2}{2} \left\langle \boldsymbol{J}^2 - \boldsymbol{L}^2 - \boldsymbol{S}^2 \right\rangle \tag{2.5}$$

$$= \frac{\gamma \hbar^2}{2} \left[j(j+1) - l(l+1) - s(s+1) \right] \tag{2.6}$$

The spin-orbit perturbation leads to a splitting between the $j_h = \frac{3}{2}$ and the $j_h = \frac{1}{2}$ states. For GaAs, the splitting is $E_{so} \sim 350\,\text{meV}$. The higher energy holes in the $j_h = \frac{1}{2}$ states occupy the split-off (SO) band and for the most part do not contribute strongly to the electrical or optical properties of GaAs. In bulk GaAs, the remaining states are degenerate at the zone center and their dispersion has different curvature depending on m_h. Correspondingly they are called the light hole (LH) and the heavy hole (HH) states accordingly. However, in quantum wells (QWs), at $k = 0$ the heavy hole and light hole states split because of symmetry breaking in the direction $\perp$ to the QW plane.

Excitons within GaAs QWs are formed by electrons binding to both heavy and light holes, leading to LH excitons and HH excitons. The energy difference between these different exciton species is $> 15\,\text{meV}$ for the experiments presented in this dissertation. The HH exciton has the lower energy and is the type examined throughout this dissertation.

When the electron and hole bind to form a HH exciton, the angular momentum state of the exciton is given by the combined angular momentum of the underlying electrons and holes $\boldsymbol{J}_X = \boldsymbol{J}_e + \boldsymbol{J}_h$. In this manner, the z-components of the electron and hole spin add to give the full set of spin states available to the HH exciton as $m_X \in \pm 1, \pm 2$. To conserve angular momentum, only excitons in the $m_X = \pm 1$ states are able to recombine through a first order process, emitting a photon in the z direction, perpendicular to the CQW plane. Hence, these bright exciton states are the primary source of the experimentally observed exciton PL from GaAs QWs.

2.3 Indirect excitons

Experimental measurements of the quantum degenerate exciton gases predicted by theory rely on the successful production of exciton gases that can cool to the lattice temperature before recombination. Semiconductor crystal lattices can be routinely cooled to temperatures well below 1 K in He dilution refrigerators. However, it is experimentally challenging to lower the temper-

ature of the exciton gas to even a few Kelvin. The exciton temperature T_X is determined by the ratio of the energy relaxation rate and the recombination rate for excitons in the system. In order to create a cold exciton gas with T_X close to the lattice temperature, the exciton lifetime should considerably exceed the exciton energy relaxation time. Additionally, for the study of degenerate exciton gases, the ground state of the system must be an excitonic state instead of the metallic electron-hole liquid, which is the ground state for Si and Ge, and is a large obstacle for the creation of exciton gases in these materials [Keldysh, 1986].

Historically, efforts to observe quantum degenerate exciton gases focused primarily on bulk semiconductors, with Cu_2O and CuCl [Hulin et al., 1980; Snoke et al., 1987, 1990; Hasuo et al., 1993; Fortin et al., 1993; Lin & Wolfe, 1993; Mysyrowicz et al., 1996; Goto et al., 1997; O'Hara et al., 1999a,b; Warren et al., 2000; O'Hara & Wolfe, 2000], as well as uni-axially strained Ge [Kukushkin et al., 1981; Timofeev et al., 1983] serving as the primary material systems investigated. In Cu_2O, the ground state is optically inactive leading to a low recombination rate, while in strained Ge it was proposed that the stability of the electron-hole liquid is reduced by the strain, enabling the formation of excitons in place of the metallic electron-hole liquid found in unstrained Ge. The results of research into these materials exposed many difficulties in achieving the sufficiently cold and dense exciton gases required for condensation.

As a result of the difficulties in producing sufficiently cold and dense gases of excitons in bulk material systems, alternative schemes focusing on quasi two dimensional (2D) gases of excitons in quantum wells (QWs) have been under considerable attention for over a decade. In specific, indirect excitons, formed from electrons and holes that are spatially separated into two neighboring coupled quantum wells (CQWs) by an electric field applied perpendicular to the plane of the QWs, have a number of properties which are ideal for the study of degenerate exciton gases. An example of the bandgap energy structure for semiconductor CQWs is shown in Figure 2.2. The separation of the electron and hole wavefunctions into separate neighboring QWs causes a significant reduction in the exciton recombination rate [Lozovik & Yudson, 1976; Shevchenko,

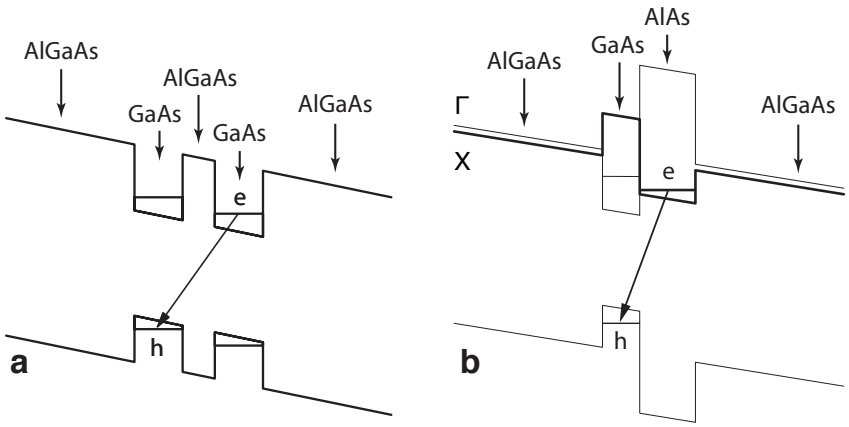

Figure 2.2: a) Energy bandgap structure for symmetric GaAs CQWs embedded in insulating $Al_xGa_{1-x}As$. b) Energy bandgap structure for coupled GaAs and AlAs QWs embedded in $Al_xGa_{1-x}As$, where the energy-gap minimum for electron occurs at the X point in the wider AlAs QW.

1976; Fukuzawa et al., 1990]. This in turn leads to a radiative exciton lifetime for indirect excitons that is three to six orders of magnitude greater than for direct excitons confined to a single QW. Additionally, exciton cooling efficiency is drastically enhanced when excitons are placed into QWs. The confinement in one dimensional leads to a relaxation of the momentum conservation law along the z direction, the direction perpendicular to the QW plane. In bulk semiconductors, the ground-state mode $E = 0$ couples only to a single longitudinal acoustic (LA) phonon energy state $E = E_0 = 2M_X v_s^2$, where v_s is the sound velocity. However, in quasi-2D systems, such as QWs, because of the relaxed momentum conservation in the z direction, the ground-state mode $E = 0$ is coupled to the continuum of energy states $E \geq E_0$ [Tikhodeev, 1989, 1990; Ivanov et al., 1997; Zhao et al., 1997; Ivanov et al., 1999].

An indirect exciton is a dipole oriented perpendicular to the QW plane. This repulsive dipolar interaction between the indirect excitons stabilizes the exciton state against formation of metallic electron-hole droplets [Yoshioka & MacDonald, 1990; Zhu et al., 1995; Lozovik & Berman, 1996], leading to an

excitonic ground state. Additionally, the repulsive interaction results in effective screening of the in-plane disorder potential that arises from interface defects inherent in the QW growth [Ivanov, 2002]. The dipolar character of the indirect excitons and resulting shifts in energy with changes in density allow for local determination of the exciton density.

In addition to the advantageous cooling properties and long lifetimes of quasi-2D indirect excitons, the system is ripe with opportunities for finely tuned *in-situ* manipulations of the exciton energy landscape. Because of the dipole character, an externally applied electric field provides direct control of the exciton energy. By spatially patterning the applied electric fields is possible to create virtually arbitrary energy landscapes for the excitons.

2.4 Pattern formation of excitons

Spatially resolved investigation of the photoluminescence (PL) from indirect excitons in CQWs has lead to the observation of a rich field of patterns that form in the exciton PL. Under low intensity excitation by a tightly focused laser spot the exciton PL follows the shape of the laser excitation very closely. However, with increasing excitation power at photon energies above the bandgap for the barrier material surrounding the CQWs, the exciton PL is characterized by two concentric rings surrounding the excitation spot (see Figure 2.3) [Butov et al., 2002]. The area surround the rings is dark, yet the region between rings is filled with localized bright spots. The inner ring radius reaches tens of microns, while the external ring radius can easily exceed 100 μm. The radii of both rings are determined by the applied voltage and laser excitation power. For sufficiently low temperatures, the external ring becomes fragmented into an array of macroscopically ordered beads with a well defined period [Butov et al., 2002; Yang et al., 2006], this state has been named the macroscopically ordered exciton state (MOES).

For both excitation above the insulating AlGaAs bandgap and at resonant excitation, most of the photo-generated electrons and holes cool and form exci-

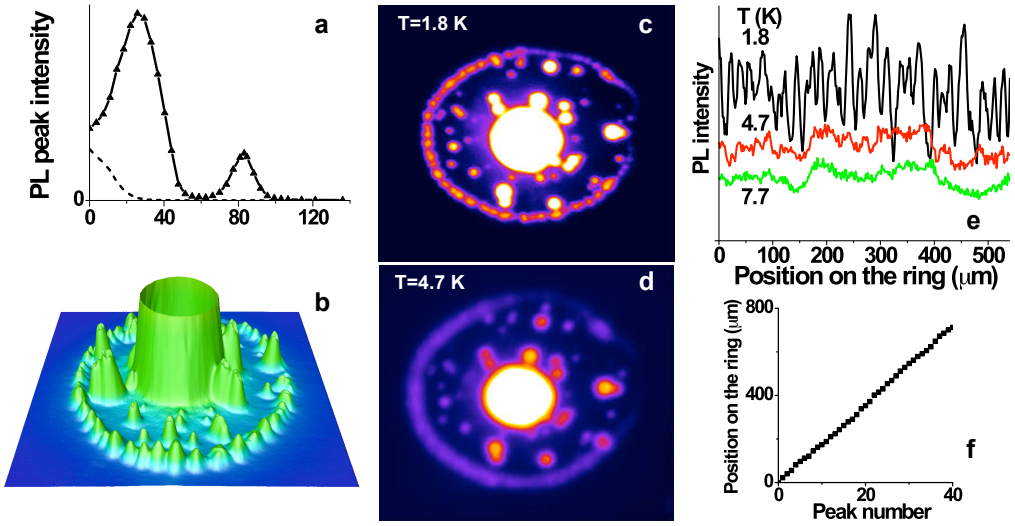

Figure 2.3: (a) Peak intensity of the indirect exciton PL vs r, the distance from the excitation spot center, at $T = 1.8$ K, $V_g = 1.22$ V, and the excitation power $P_{ex} = 690$ μW. The excitation spot profile is shown by the dashed line. Spatial pattern of the indirect exciton PL intensity at $T = 1.8$ (c) and 4.7 K (d) for $P_{ex} = 690$ μW. The area of view is 475×414 μm. (e) The corresponding variation of the indirect exciton PL intensity along the external ring at $T = 1.8$, 4.7, and 7.7 K. The dependence of the position of the indirect exciton PL intensity peaks along the external ring vs the peak number is nearly linear (f), showing that the fragments form a periodic chain. (b) 3D plot of the PL pattern at $T = 380$ mK, $V_g = 1.24$ V, and $P_{ex} = 930$ μW. From [Butov et al., 2002; Butov, 2004].

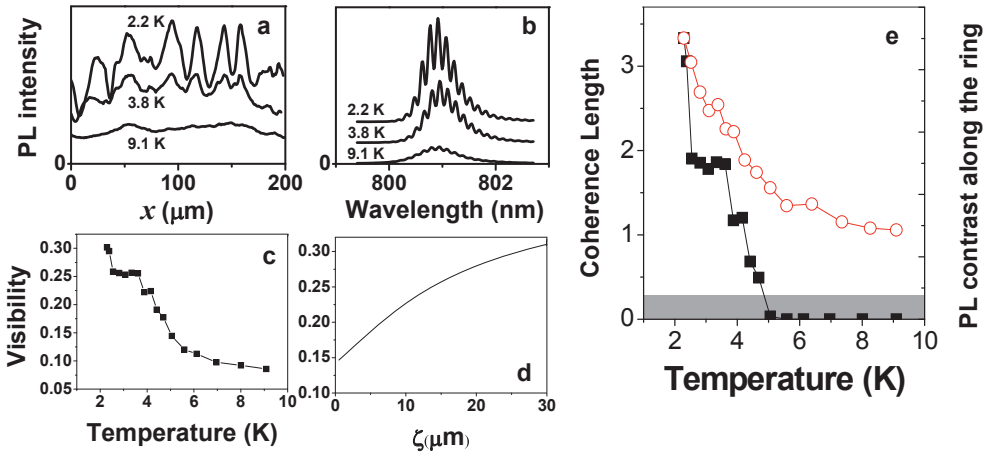

Figure 2.4: (a) Variation of the indirect exciton PL intensity along the external ring at $T = 2.2$, 3.8 and 9.1 K. (b) Interference profiles at $T = 2.2$, 3.8 and 9.1 K. (c) Visibility of the interference fringes vs T. (d) Calculated visibility as a function of the coherence length. (e) The exciton coherence length (squares) and contrast of the spatial intensity modulation alond the ring (circles) vs T. The shaded area is beyond experimental accuracy. $V_g = 1.24$ V, $P_{ex} = 0.7$ mW for all the data. From [Yang et al., 2006; Fogler et al., 2008].

tons within the region near the laser excitation spot. The steady state dynamics of thermalization, generation, and recombination of excitons formed near to the laser excitation spot leads to the inner ring observed in the exciton PL. A detailed description of this process will be laid out in the following chapter. In contrast to the inner ring, the outmost ring and the localized bright spots are observed only for excitation at energies above the AlGaAs barrier bandgap energy. They have been explained within a classical framework by macroscopic charge separation of electrons and holes within the CQW [Butov, 2004; Rapaport et al., 2004; Yang et al., 2010]. The charge neutrality of the gas of electrons, holes, and excitons present within the CQW when the sample is excited by above bandgap laser excitation is generally violated primarily by differences in the collection efficiencies of electrons and holes to the CQW [Zrenner et al., 1990]. For the typical voltages applied to the sample in the indirect exciton regime, there is a small but persistent current of electrons through the sample that leads to the creation of an electron gas within the CQW. Under laser excitation excess holes are injected to the CQWs in the excitation spot due to the higher collection efficiency of the photoexcited holes to the CQW, given their larger effective mass. The excess holes created in the excitation spot diffuse outward and recombine with electrons leading to a depletion of electrons near the region of laser excitation. This leads to the formation of an essentially electron free region, allowing the excess holes to travel large distances before meeting an electron. At the same time, a counter flow of electrons towards the laser spot is established. In regions at the interface of the hole and electron rich regions, excitons are formed, leading to both the external ring and localized bright spots. The external ring is formed at the interface between the central hole rich region surrounding the laser and the outer electron rich region. The localized bright spots are essentially smaller versions of the external ring that form near the electron current filaments flowing through the sample perpendicular to the CQW. Observation of the external ring up to high temperatures is expected as it does not require degeneracy within the system.

The most intriguing feature in the patterns is the temperature dependent

fragmentation of the external ring. Though the external ring is a classical object by itself, given its large distance from the heat sources in the sample, both the laser excitation spot and electron current filaments, it is also the region where the coldest exciton gas is created. The MOES is a new unpredicted phenomenon and experimental and theoretical work to understand its origin is underway. The explanation consistent with the experimental data explains the MOES in terms of quantum degeneracy of the excitons at low temperatures. An instability with a periodic 1D pattern can be formed by the stimulated kinetics of exciton formation below a critical temperature [Levitov et al., 2005]. The model is in qualitative agreement with observations. The driving interaction is that the creation of additional excitons, which are Bose particles, is more probable in region of higher exciton density. This dynamic instability leads to the build up of a spatially periodic density modulation in the exciton gas. The formation of the MOES occurs in concert to a significant increase in the coherence length of excitons in the system, as measured by optical interferometry (see Figure 2.4). This increase in the coherence indicates the formation of a condensate in k-space.

The build up of quantum coherence in a Bose gas of excitons is not a feature unique to the excitons within the external ring. For sufficient control of the temperature and density of the excitons within the CQWs, quantum degenerate phenomena should be observable in any regions with sufficiently high density and sufficiently low enough temperature. A comprehensive understanding of the exciton transport, generation, recombination, and thermalization processes has lead to the possibility for techniques to control excitons within the system and to form virtually arbitrary regions of cold and dense exciton gases. A general purpose model for the evolution of exciton gases combined with various experimental techniques for exciton control comprises the core of the dissertation.

3 Experimental methods and sample structure

3.1 Methods for spatially resolved spectroscopy

In the experiments, both spatially resolved x-y images and spatially resolved spectra E-y images are collected. The exciton photo-luminescence (PL) is collected by a Mitotoyo objective with numerical aperture of 0.28 leading to a spatial resolution of $\lesssim 1.4\,\mu$m. The x-y PL pattern is imaged by a nitrogen-cooled CCD camera with the spectral selection by an interference filter adjusted to the indirect exciton energy. Fine adjustment of the filtering energy is done by rotating two interference filters relative to the optical axis. For the spatially resolved spectra, the CCD camera is placed after a spectrometer to acquire E-y images of the exciton PL.

For time resolved measurements, a PicoStar HR TauTec intensifier with a time-integration window of $\delta t = 4\,$ns was used to acquire both the spatial, x-y, and spectral, E-y, PL images at varied delay time t. The timing information was captured by placing the time-gated intensifier before the CCD. The time resolved images presented are the result of integrating numerous time slices into one composite exposure showing the state of the exciton PL after a fixed delay time from the onset of a laser excitation pulse. The spectral diffraction and time-gated imaging combined allow the direct visualization of the evolution of the indirect exciton PL intensity and energy as a function of delay time t

A schematic of the experimental setup is shown in Figure 3.1.

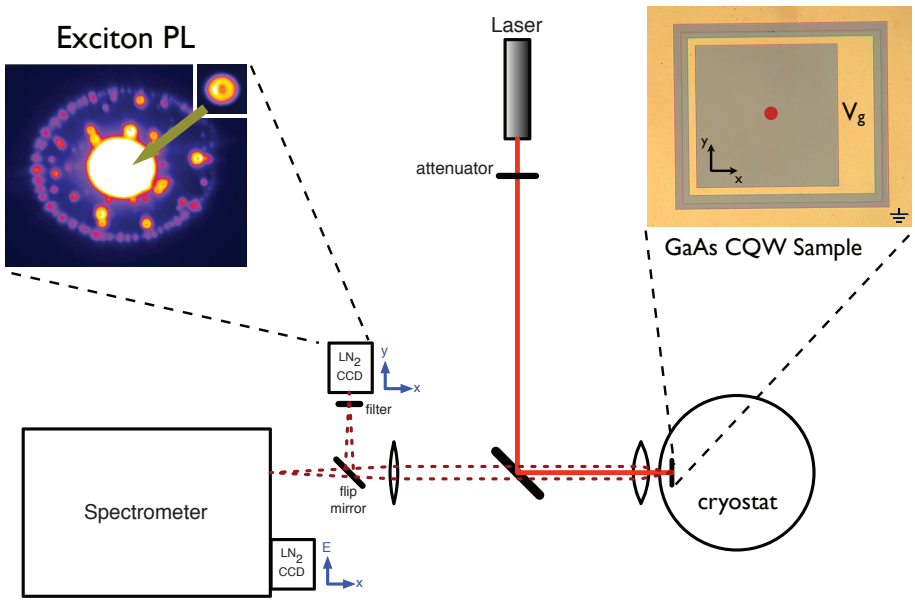

Figure 3.1: The spatial *x*-*y* exciton PL pattern is imaged by a nitrogen-cooled CCD camera with the spectral selection by an interference filter adjusted to the indirect exciton energy. Fine adjustment of the filtering energy is done by rotating the angle of incidence for two interference filters. The *E*-*x* information is collected after being dispersed by an optical diffraction grating spectrometer.

3.2 CQW sample structure

The CQW structures used in these experiments were grown by molecular beam epitaxy onto Si doped GaAs wafers. The bottom electrode layer is created by a deposited layer of degenerately doped n+-GaAs, $N_{\mathrm{Si}} = 10^{18}\,\mathrm{cm}^{-3}$. The CQWs are positioned within a barrier layer of $\mathrm{Al}_x\mathrm{Ga}_{1-x}\mathrm{As}$. Two types of CQWs are considered in this dissertation, the first contains two 8 nm GaAs QWs separated by a 4 nm $\mathrm{Al}_{0.33}\mathrm{Ga}_{0.67}\mathrm{As}$ barrier, the second type is created by a 2.5 nm GaAs layer placed directly in contact with a 4 nm AlAs layer (see Figure 3.2).

For the samples used to study exciton transport and pattern formation, the sample is capped with n+-GaAs and the CQWs are placed 200 nm from both the uniform top gate and the uniform back gate. The back gate is contacted by etching into the mesa before depositing gold contact pads.

For the samples used to study exciton control, the sample is capped with undoped GaAs, onto which laterally pattern electrodes are deposited. A variety of electrodes, including non-transparent thick Au (used for proof of principle work in chapter 6), as well as semitransparent thin film Pt/Au, and indium tin oxide (ITO) have been used in exciton control studies. In CQW samples for exciton control, the CQWs are placed 100 nm from the uniform back gate, within a 1 μm thick barrier layer.

Indirect excitons in the CQW structure are formed from electrons and holes confined to different QWs. Separation between the electron and hole layers in the CQW structure causes the optical lifetime τ_{opt} of the indirect excitons to exceed that of regular direct excitons by orders of magnitude.

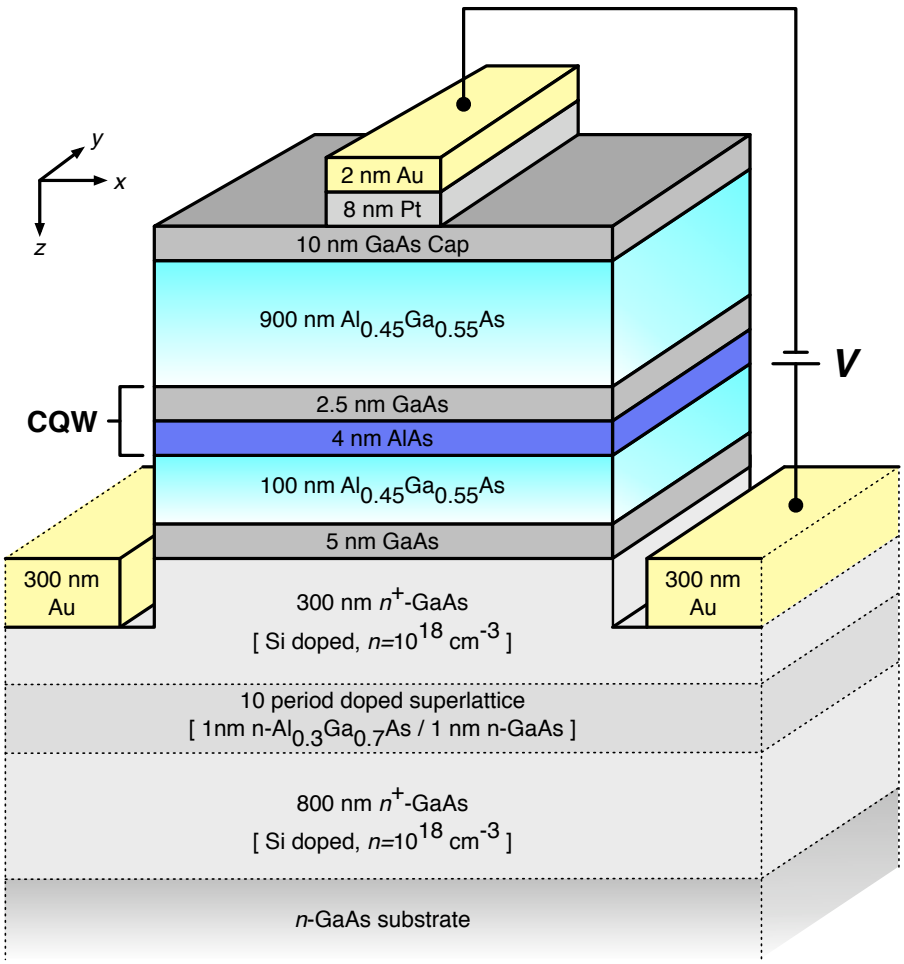

Figure 3.2: The illustration shows a typical layer structure of the CQWs used for electrostatic control of indirect excitons. Critically, the CQW layer is placed significantly closer to the ground plane, which reduces the in-plane electric field that can lead to exciton dissociation.

4 Exciton transport and thermalization

4.1 Origin of the exciton inner ring

4.1.1 Introduction

More than two decades ago, long-distance diffusion and drift transport of charge-neutral excitons with a long lifetime was optically visualized in bulk Si and Cu_2O [Tamor & Wolfe, 1980; Trauernicht et al., 1984]. In these earlier works, strain gradient potential traps were used to induce the drift motion. Due to the low particle concentrations, the transport was described in terms of a classical picture, with no quantum-statistical corrections. The diffusion coefficient was determined by exciton-phonon scattering. In-plane propagation of long-lived indirect excitons in coupled QWs over large distances has also been reported [Hagn et al., 1995; Butov & Filin, 1998; Larionov et al., 2000; Butov et al., 2002; Vörös et al., 2005; Ivanov et al., 2006; Gärtner et al., 2006, 2007; Vögele et al., 2009]: in this case one has a unique possibility to optically map the quasi-two-dimensional motion of composite bosons. Furthermore, the density n_{2d} of indirect excitons can be large enough to ensure nonclassical population of the ground-energy state, $N_{E=0} = e^{T_0/T} - 1 \gtrsim 1$, where $T_0 = (\pi\hbar^2 n_{2d})/(2k_B M_x)$ and T are the degeneracy temperature and exciton temperature, respectively, and M_x is the exciton in-plane translational mass. Furthermore, the built-in dipole moment of an indirect exciton, $e{\cdot}d$, allows control of exciton transport by electrode voltages [Hagn et al., 1995; Gärtner et al., 2006; High et al., 2008, 2009b,a;

Remeika et al., 2009] (d is the separation between the electron and hole layers). The combination of long lifetime, large transport distance, efficient cooling, and an ability to control exciton transport makes the indirect excitons a model system for the investigation of in-plane transport of quasi-two-dimensional (quasi-2D) cold Bose gases in solid state materials.

One of the most striking features of photoluminescence associated with indirect excitons is the appearance of two *PL rings* [Butov et al., 2002]. While the second, external ring has already been explained in terms of in-plane spatially separated electrons and holes [Butov, 2004; Rapaport et al., 2004], the origin of the inner ring, which arises purely due to the transport of indirect excitons, remained unclear. The proposed explanation for the ring is that in the optically-pumped area the exciton temperature T is much larger than the lattice temperature $T_{\rm b}$. As a result, the optical decay of excitons is suppressed, but while they diffuse out they cool down and eventually become optically-active, giving rise to a local increase of the PL signal.

In this section we present a steady state microscopic theory for the long-range transport, thermalization and optical decay of QW excitons, model the inner PL ring, and show an effective screening of QW disorder for $n_{\rm 2d} \gtrsim 10^{10}$ cm^{-2} [Ivanov et al., 2006]. By numerically fitting the PL spectra we clarify the main scattering channels which contribute to the diffusion of indirect excitons and evaluate the diffusion coefficient and amplitude of the QW disorder potential. In the proposed model, the exciton temperature T is affected by heating due to the optical excitation, heating due to the LA-phonon assisted conversion of the mean-field energy into the internal energy, and recombination heating or cooling due to the optical decay of low-energy excitons. The mean-field energy of indirect excitons also gives rise to a potential energy gradient and, therefore, to the in-plane drift motion. Our analysis shows that the inner ring is a generic feature of cw photoluminescence from excitons, direct or indirect, in high-quality QWs.

4.1.2 Experimental methods

Using the steady state collection technique described in section 3.1, we observe a two-dimensional spatial image of the inner ring (see Figure 4.1a, c, and d). Note that the inner PL ring can be missed if the bulk emission is not removed from the PL signal. In Figure 4.1e and f we plot the measured exciton PL in the *energy-coordinate* plane. The exciton energy $E_{\rm PL}$ decreases with increasing distance from the excitation spot, as detailed below. This results in an arrow-shaped profile of the exciton PL images in the *E-x* coordinates. The external ring is also seen at high excitations, both in *x-y* (Figure 4.1a) and *E-x* (Figure 4.1e) coordinates. The excitation is done by a HeNe laser at 633 nm (the laser spot is a Gaussian with FWHM = $2\sigma \simeq 6\,\mu$m, the excitation power $P_{\rm ex} = 1 - 400\,\mu$W). The coupled QW structure with two 8 nm GaAs QWs separated by a 4 nm $Al_{0.33}Ga_{0.67}As$ barrier is grown by molecular beam epitaxy (see section 3.2).

4.1.3 Exciton transport model

A set of coupled nonlinear differential equations we use in order to model transport, thermalization, and photoluminescence of indirect excitons is given by

$$\frac{\partial n_{\rm x}}{\partial t} = \nabla\Big[D_{\rm x}\nabla n_{\rm x} + \mu_{\rm x} n_{\rm x}\nabla\left(u_0 n_{\rm x} + U_{\rm QW}\right)\Big] - \Gamma_{\rm opt} n_{\rm x} + \Lambda_{\rm x}\,, \tag{4.1}$$

$$\frac{\partial T}{\partial t} = \left(\frac{\partial T}{\partial t}\right)_{n_{\rm x}} + S_{\rm pump} + S_{\rm opt}\,, \quad \text{where}$$

$$\left(\frac{\partial T}{\partial t}\right)_{n_{\rm x}} = -\frac{2\pi}{\tau_{\rm sc}}\left(\frac{T^2}{T_{\rm dB}}\right)\left(1 - e^{-T_{\rm dB}/T}\right)\int_1^\infty d\varepsilon\ \varepsilon\sqrt{\frac{\varepsilon}{\varepsilon-1}} \times\frac{\left|F_z\left(a\sqrt{\varepsilon(\varepsilon-1)}\right)\right|^2}{\left(e^{\varepsilon E_0/k_{\rm B}T_{\rm b}} - 1\right)}\ \frac{e^{\varepsilon E_0/k_{\rm B}T_{\rm b}} - e^{\varepsilon E_0/k_{\rm B}T}}{\left(e^{\varepsilon E_0/k_{\rm B}T} + e^{-T_{\rm dB}/T} - 1\right)}\,, \tag{4.2}$$

$$I_{\rm PL}^{\rm sig} = \Gamma_{\rm opt}^{\rm sig} n_{\rm x}\,, \quad \text{where}$$

$$\Gamma_{\rm opt}^{\rm sig} = \frac{1}{2\tau_{\rm R}}\left(\frac{E_\gamma}{k_{\rm B}T_{\rm dB}}\right)\int_{z_{\rm s}}^1 \frac{1+z^2}{[(e^{E_\gamma/k_{\rm B}T})/(1-e^{-T_{\rm dB}/T})]e^{-z^2E_\gamma/k_{\rm B}T} - 1}\ dz\,. \tag{4.3}$$

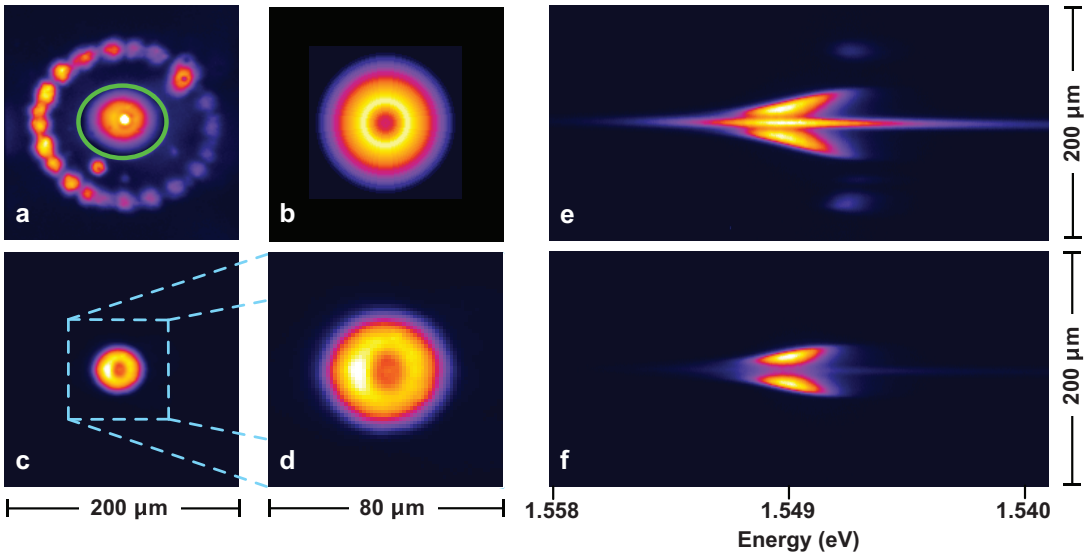

Figure 4.1: (a), (c)-(f) Experimental and (b) calculated patterns of the PL signal from indirect excitons. In (a), the PL intensity in the area within the green circle is reduced by a constant factor for better visualization. A bright spot in the middle of the inner ring shown in (a) is due to residual bulk emission. (e) and (f) Image of the PL signal in the E-x coordinates. The external PL ring is also seen for high excitations, both in (a) x-y and (e) E-x coordinates. For (a) and (e) the excitation power is $P_{\mathrm{ex}} = 402\,\mu\mathrm{W}$ and for (b)-(d) and (f) $P_{\mathrm{ex}} = 101\,\mu\mathrm{W}$, respectively, and $T_{\mathrm{b}} = 1.5\,\mathrm{K}$.

Equation 4.1-4.3 describe in-plane profiles of the density $n_x = n_x(r,t)$, effective temperature $T = T(r,t)$ and signal PL intensity $I_{PL}^{sig} = I_{PL}^{sig}(r,t)$ of indirect excitons.

In the drift-diffusion Equation 4.1 for in-plane transport of the particles [Ivanov, 2002], D_x, μ_x, Γ_{opt}, and Λ_x are the diffusion coefficient, mobility, radiative decay rate, and generation rate of indirect excitons, respectively. The ∇-operator has only the radial component, $\nabla_r = \partial/\partial r$, due to the cylindrical symmetry one deals with. The mobility μ_x is given in terms of the diffusion coefficient D_x through the generalized Einstein relationship, $\mu_x = D_x[(e^{T_{dB}/T} - 1)/(k_B T_{dB})]$ [Ivanov, 2002]. The random potential $U_{QW} = U_{rand}(\mathbf{r})$ on the right-hand side (r.h.s.) of Equation 4.1 is mainly due to the CQWs thickness and alloy fluctuations. The drift term $\propto \nabla(u_0 n_x + U_{QW})$ stems from the dipole-dipole interaction of indirect excitons and the in-plane potential U_{QW}. For the first contribution we use $u_0 = 4\pi d(e^2/\varepsilon_b)$, ε_b is the background dielectric constant, and d is the separation between electron and hole layers. This corresponds to the mean-field approximation of the interaction energy of indirect excitons. The latter stems from the dipole-dipole repulsion between the particles and gives rise to the blue shift of the PL line [Yoshioka & MacDonald, 1990; Butov et al., 1994; Zhu et al., 1995]. The mean-field energy gives rise to the in-plane drift motion with the velocity $\mathbf{v}_{drift} = -\mu_x u_0 \nabla n_x$. As a result, an effective screening of the disorder potential U_{rand} by dipole-dipole interacting indirect excitons builds up with increasing n_x [Ivanov, 2002; Zimmermann, 2005]: the excitons tend to accumulate near the minima of $U_{rand}(\mathbf{r})$ [local increase of $u_0 n_x(\mathbf{r})$] and avoid the maxima of $U_{rand}(\mathbf{r})$ [local decrease of $u_0 n_x(\mathbf{r})$]. As we show below, in our high-quality structures $U^{(0)} = 2\langle|U_{rand}(\mathbf{r})|\rangle \simeq 0.9\,\text{meV}$ and the mean-free energy $u_0 n_x^{(0)} \simeq 1.6\,\text{meV}$ for $n_x^{(0)} = 10^{10}\,\text{cm}^{-2}$, so that at low exciton temperatures $T \sim 1\,\text{K}$ the QW disorder is strongly screened and practically removed for $n_x \gtrsim n_x^{(0)}$. For $n_x \gtrsim 10^9\,\text{cm}^{-2}$ relevant to the experiments, the correlation energy of exciton-exciton interaction is less than the mean-field energy and therefore is neglected in the present model. The radiative rate $\Gamma_{opt} = 1/\tau_{opt}$ on the r.h.s. of Equation 4.1 is $\Gamma_{opt} = \Gamma_{opt}^{sig}(z_s = 0)$ with Γ_{opt}^{sig} given by Equation 4.3.

The first term on the r.h.s. of Equation 4.2, $(\partial T/\partial t)_{n_x}$, describes thermalization (cooling) of indirect excitons, due to their interaction with a bath of bulk acoustic phonons at temperature T_b [Ivanov et al., 1999]. Here, $\tau_{sc} = (\pi^2\hbar^4\rho)/(D_{dp}^2 M_x^3 v_{LA})$ is the characteristic scattering time, $E_0 = 2M_x v_{LA}^2$ is the characteristic energy of the longitudinal acoustic (LA) phonon assisted thermalization at low temperatures, v_{LA} is the velocity of long-wave-length LA phonons, ρ is the crystal density, and $D_{dp} = D_c - D_v$ is the deformation potential of exciton – LA-phonon interaction. The form-factor $F_z(a\sqrt{\varepsilon(\varepsilon-1)})$ refers to a rigid-wall confinement potential of quantum wells, where $a = (d_{QW} M_x v_{LA})/\hbar$ with d_{QW} the quantum well thickness and $\varepsilon = E/E_0$ the normalized single-particle kinetic energy of excitons, and $F_z(\chi) = [\sin(\chi)/\chi][e^{i\chi}/(1-\chi^2/\pi^2)]$. The terms S_{pump} and S_{opt} on the r.h.s. of Equation 4.2, which are detailed in Ivanov [2004], deal with heating of indirect excitons by the laser pulse and recombination heating or cooling of the particles. The laser-induced heating is given by

$$S_{pump} = \frac{E_{inc} - k_B T\, I_2}{2k_B T\, I_1 - k_B T_{dB} I_2}\, \Lambda_x^{T_{dB}}\,, \tag{4.4}$$

where $\Lambda_x^{T_{dB}} = [(\pi\hbar^2)/(2k_B M_x)]\Lambda_x(r,t)$ and $E_{inc} \gg k_B T_b$ is an average kinetic energy of high-energy indirect excitons injected into the CQW structure by means of photocarriers. The latter are generated in the GaAs and AlGaAs layers by the laser pulse. The term S_{opt}, which takes into account a contribution from the "optical evaporation" of low-energy indirect excitons to the total energy balance [Ivanov, 2004], is determined by

$$S_{opt} = \frac{k_B T\, I_2 \Gamma_{opt} - E_\gamma \Gamma_{opt}^E}{2k_B T\, I_1 - k_B T_{dB} I_2}\, T_{dB}\,. \tag{4.5}$$

Here, the energy rate Γ_{opt}^E, due to the optical decay, is given by

$$\Gamma_{opt}^E = \frac{1}{2\tau_R}\left(\frac{E_\gamma}{k_B T_{dB}}\right)\int_0^1 \frac{1-z^4}{[(e^{E_\gamma/k_B T})/(1-e^{-T_{dB}/T})]e^{-z^2 E_\gamma/k_B T} - 1}\, dz\,. \tag{4.6}$$

In Equation 4.4 and Equation 4.5, the parameters $I_{1,2} = I_{1,2}(T_{dB}/T)$ are $I_1 =$

$(1-e^{-T_{dB}/T})\int_0^\infty dz[z/(e^z+e^{-T_{dB}/T}-1)]$ and $I_2 = e^{-T_{dB}/T}\int_0^\infty dz[(ze^z)/(e^z+e^{-T_{dB}/T}-1)^2]$.

Finally, the intensity I_{PL}^{sig} of the PL signal, collected in the normal direction within an aperture angle α (in the experiment, $\alpha \simeq 30°$), is given by Equation 4.3. In this case, the lower integration limit in the expression for the decay rate Γ_{opt}^{sig} is $z_s = 1-\sin^2(\alpha/2)$ [see Equation 4.3]. Both Γ_{opt}^{sig} and Γ_{opt} are inversely proportional to the intrinsic radiative lifetime τ_R of the exciton ground-state with zero in-plane momentum.

In our model, the diffusion coefficient $D_x = (D_{x-x}D_{x-imp})/(D_{x-x}+D_{x-imp})$ has two contributions: diffusion due to scattering by imperfections (QW impurities and bulk LA-phonons), D_{x-imp}, and self-diffusion due to exciton-exciton scattering, D_{x-x}. The latter channel is important for $n_x \gtrsim 10^{10}\,cm^{-2}$ and D_{x-x} is approximated by $D_{x-x} = C_{x-x}(T/T_{dB})$ [Ivanov, 2002]. For r far away from the excitation spot, the asymptotic solution yields $I_{PL} \propto \exp[-(\Gamma_{opt}/D_{x-imp})^{1/2}r]$. In contrast, the experimental data show a much more steep decay of the PL signal and its *spatial pinning* at a critical radius $r_{cr} = r_{cr}(P_{ex})$ (e.g., $r_{cr} \simeq 40\,\mu m$ for $P_{ex} = 402\,\mu W$, see Figure 4.1a). We attribute such a behaviour to the n_x-dependent screening of long-range-correlated QW disorder by dipole-dipole interacting indirect excitons. The narrowing effect is illustrated in Figure 4.2a for a particular realization of the random potential $U_{rand}(r)$. In order to evaluate the random drift term $\mu_x n_x \nabla(U_{QW})$ on the r.h.s. of the drift-diffusion Equation 4.1, we implement a thermionic model [Ivanov, 2002; Ivanov et al., 2006]. In this approach, the influence of disorder is approximately taken into account by using the disorder-dependent effective diffusion coefficient:

$$D_x = D_x^{(0)} \exp\left[-\frac{U^{(0)}}{k_B T + u_0 n_x}\right], \tag{4.7}$$

where $D_x^{(0)}$ is the input diffusion coefficient in the absence of CQW disorder, and $U^{(0)}/2 = \langle|U_{rand}(\mathbf{r}) - \langle U_{rand}(\mathbf{r})\rangle|\rangle$ is the amplitude of the disorder potential. Equation 4.7 describes the temperature and density dependent screening of the long-range-correlated disorder potential $U_{QW} = U_{rand}(\mathbf{r})$ by dipole-dipole interacting indirect excitons. The vanishing screening at the external edge of the

inner PL ring, due to reduced exciton density, leads to a strong suppression of the exciton propagation away from the excitation spot and, as a result, to the sharp contrast of the ring [Ivanov et al., 2006].

The excess energy $E_{\rm inc}$ of a created (incoming) indirect exciton is large: it exceeds the energy splitting between the direct and indirect excitons, which is about 20 meV. For the highest generation rates used in the experiments, the exciton temperature $T^{\rm max} \simeq 6.4\,{\rm K}$ at the laser spot centre is much larger than $T_{\rm b} \simeq 1.5\,{\rm K}$.

In contrast with the evaporative cooling schemes used in atomic optics to remove high-energy atoms from magnetic traps [Cornell & Wieman, 2002; Ketterle, 2002], the optical evaporation of QW excitons is an inherent process, which deals with the lowest-energy particles, $0 \le E \le E_\gamma$, from the radiative zone. Both signs of $S_{\rm opt}$ can be realized: $S_{\rm opt} > 0$ ($S_{\rm opt} < 0$), i.e., recombination heating (cooling) of indirect excitons for $k_{\rm B}T \gtrsim E_\gamma$ and $k_{\rm B}T_0$ ($k_{\rm B}T \ll E_\gamma$ and $k_{\rm B}T_0$). In our case recombination heating occurs: far away from the excitation spot T exceeds $T_{\rm b}$ by about 3 mK. Due to the long radiative lifetime of indirect excitons and relatively high $T_{\rm b}$, the recombination heating is small. However, the effect is strong for $T_{\rm b} \sim 0.1\,{\rm K}$, when an effective recombination cooling of particles occurs [Ivanov, 2004].

In order to model the experimental results within the developed microscopic picture, we solve Equation 4.1-4.6 numerically for a steady state, cylindrically-symmetric optical excitation profile, so that the generation rate $\Lambda_{\rm x}(r,t) \equiv \Lambda_{\rm x}(r) \propto P_{\rm ex}\exp(-r^2/\sigma^2)$. The best fit for the experimental data plotted in Figure 4.2a yields $U_0 = 0.9\,{\rm meV}$, $D_{\rm x-imp} = 60\,{\rm cm^2/s}$, and $C_{\rm x-x} = 15\,{\rm cm^2/s}$. The calculated spatial profile of the PL signal, $I_{\rm PL} = I_{\rm PL}(r)$, is shown in Figure 4.2b for various pump powers $P_{\rm ex}$. While the density profile $n_{\rm x} = n_{\rm x}(r)$ always has a bell-like shape (see Figure 4.3b and the inset of Figure 4.2a), with increasing $P_{\rm ex}$ the inner PL ring develops in the $I_{\rm PL}$-profile. This is in a complete agreement with the observations. The inner ring has a classical origin, and arises due to heating of indirect excitons by the optical excitation [$S_{\rm pump}$ term in Equation 4.2]: with increasing r the exciton temperature T rapidly decreases towards $T_{\rm b}$ (see

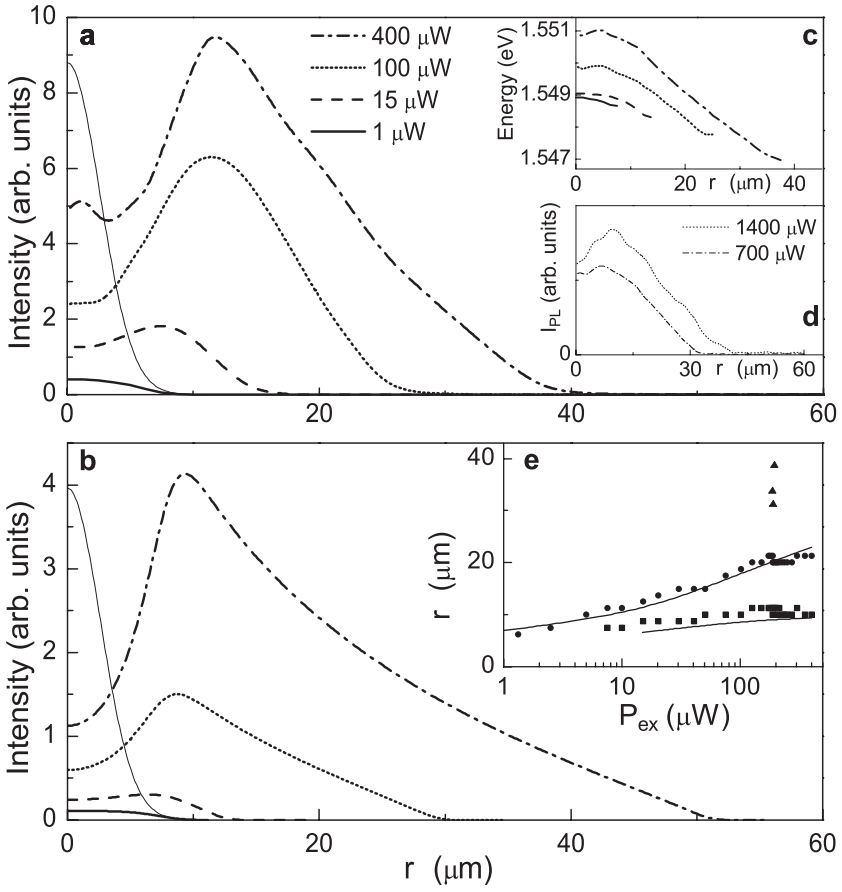

Figure 4.2: The PL intensity I_{PL}, (a) measured and (b) calculated with Equation 4.1-4.6, against radius r for four optical excitation powers P_{ex}. The Gaussian profile with of the optical excitation is shown by the thin solid lines. The cryostat temperature $T_{\mathrm{b}} = 1.5\,\mathrm{K}$. In numerical evaluations the following parameters are used: $D_{\mathrm{dp}} = 9.6\,\mathrm{eV}$, $\tau_{\mathrm{R}} = 13\,\mathrm{ns}$, $E_{\mathrm{inc}}/k_{\mathrm{B}} = 200\,\mathrm{K}$, $M_{\mathrm{x}} = 0.215\,m_0$, $d_{\mathrm{QW}} = 8\,\mathrm{nm}$, and $d = 11.5\,\mathrm{nm}$. The best fitting parameters are $U_0 = 0.9\,\mathrm{meV}$, $D_{\mathrm{x-imp}} = 60\,\mathrm{cm}^2/\mathrm{s}$, and $C_{\mathrm{x-x}} = 15\,\mathrm{cm}^2/\mathrm{s}$. (d) $I_{\mathrm{PL}} = I_{\mathrm{PL}}(r)$ of indirect excitons measured at subbarrier (780 nm)excitation for $P_{\mathrm{ex}} = 0.7\,\mathrm{mW}$ and $1.4\,\mathrm{mW}$. Bulk emission is subtracted from the total PL signal in (a) and (d). The energy position of the PL line, $E_{\mathrm{PL}} = E_{\mathrm{PL}}(r)$ for the data shown in (a) is plotted in (c). (e) The measured (square points) and calculated (solid line) inner ring radius r_{rg} *vs.* P_{ex} (the triangular points refer to the external PL ring), and the measured (circle points) and calculated (solid line) HWHM spatial extension of the PL signal against r.

Figure 4.3b); as a result, the optical lifetime $\tau_{opt} = 1/\Gamma_{opt}$ decreases too (see the inset of Figure 4.3b), giving rise to a local increase of $I_{PL}(r)$ at $r = r_{rg}$. Thus the steady state character of the inner ring is a spatial counterpart of the PL-jump observed in the time-resolved experiments [Butov et al., 2001]. Our numerical simulations also reproduce the observed increase of r_{rg} and the spatial extension of the PL area (HWHM of the signal) with increasing P_{ex} (see the inset of Figure 4.2b).

The finding of the fitting parameters, which refer to the total diffusion coefficient $\tilde{D}_x$, is *complex*, i.e., we fit all the curves plotted in Figure 4.2a [$I_{PL} = I_{PL}(r)$ and $E_{PL} = E_{PL}(r)$ for various P_{ex}] by using the same values of U_0, D_{x-imp}, and C_{x-x}. The blue shift $\delta_{PL} \geq 0$ of the PL energy E_{PL} is due to the mean-field interaction energy of indirect excitons, $\hbar\delta_{PL} = u_0 n_x$ (see the inset of Figure 4.2a). Thus we use the measured δ_{PL} to estimate the concentration $n_x^{max}(r = 0)$, and therefore the generation rate $\Lambda_x(r = 0)$, necessary for numerical modelling with Equation 4.1-4.6. The amplitude of the disorder potential, U_0, determines the steepness of $I_{PL}(r > r_{rg})$ and dependence $r_{cr} = r_{cr}(P_{ex})$ of the PL pinning radius. In turn, D_{x-imp} and C_{x-x} determine the ring contrast and $r_{rg} = r_{rg}(P_{ex})$ dependence. The total diffusion coefficient $\tilde{D}_x = \tilde{D}_x(r)$ is plotted in Figure 4.3d.

In Figure 4.3c we show that for the small size excitation spot ($\sigma \simeq 3\,\mu$m) used in the experiments, the drift velocity v_{drift}, due to the gradient of the mean-field interaction energy $u_0 n_x(r)$, is much larger than the diffusion velocity v_{diff}. The total velocity has a maximum value $v_{tot}^{max}(r \simeq r_{rg}) \simeq 1.5 \times 10^5$ cm/s for $n_x^{max}(r = 0) \simeq 2.5 \times 10^{10}\,\text{cm}^{-2}$ (see Figure 4.3c). Note that in our case the mean-field energy gradient $u_0|\nabla n_x(r \simeq r_{rg})| \simeq 1.6$ eV/cm exceeds the maximum potential gradient $|\nabla U| \simeq 0.4$ eV/cm in the strain-induced traps used in the experiments [Tamor & Wolfe, 1980; Trauernicht et al., 1984].

Finally, we emphasize that in our experiments, which deal with the cryostat temperature $T_b = 1.5$ K, nonclassical occupation numbers of modest values, $N_{E=0}^{max}(r \simeq r_{rg}) \simeq 1$, build up at the position of the inner ring (see the inset of Figure 4.3c). As illustrated in Figure 4.3c, in this case the quantum statistical corrections, e.g., to v_{diff} and to the Einstein relationship, are about 35% and therefore

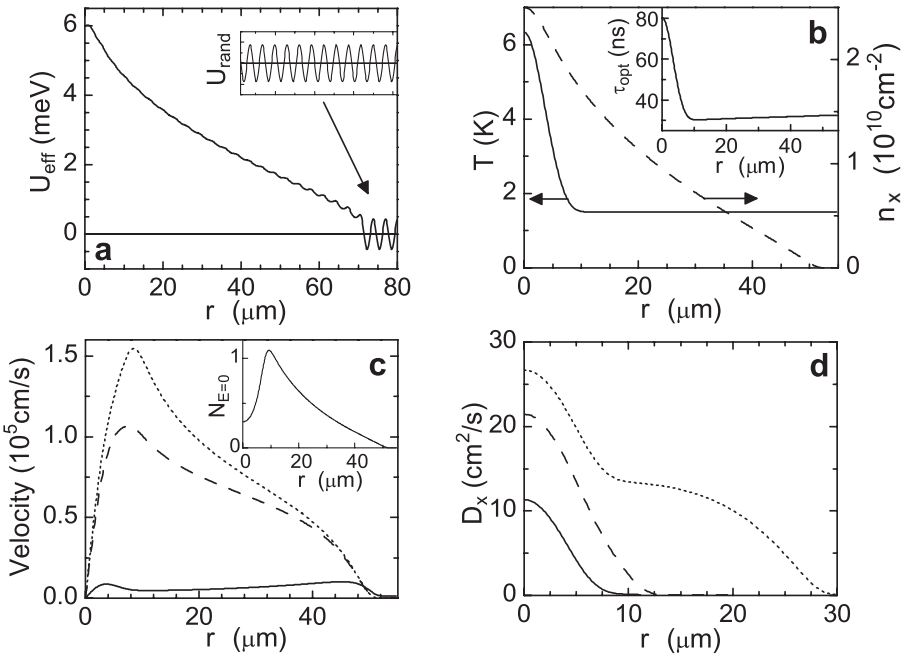

Figure 4.3: (a) The narrowing effect: screening of the long-range-correlated disorder potential $U_{\rm rand}(\mathbf{r})$ by dipole-dipole interacting indirect excitons. The QW effective potential $U_{\rm eff}(r) = U_{\rm rand}(r) + u_0 n_{\rm x}(r)$ calculated with Equation 4.1-4.6 for harmonic $U_{\rm rand}(r)$ with $U_0/2 = 0.45$ meV (see the inset). (b) $T = T(r)$ (solid line) and $n_{\rm x} = n_{\rm x}(r)$ (dashed line). Inset: $\tau_{\rm opt} = \tau_{\rm opt}(r)$. (c) Diffusion velocity $v_{\rm diff} = v_{\rm diff}(r)$ (solid line) and drift velocity $v_{\rm drift} = v_{\rm drift}(r)$ without (dashed line) and with (dotted line) quantum-statistical corrections. Inset: $N_{E=0} = N_{E=0}(r)$. Plots (a)-(c) refer to the maximum excitation, $n_{\rm x}^{\rm max} = 2.5\times10^{10}$ cm^{-2} (see the solid lines in Figure 4.2). (d) Diffusion coefficient $D_{\rm x} = D_{\rm x}(r)$ for $n_{\rm x}^{\rm max} = 0.16\times10^{10}$ cm^{-2} (solid line), 0.44×10^{10} cm^{-2} (dashed line), and 1.27×10^{10} cm^{-2} (dotted line). These values of $n_{\rm x}^{\rm max}$ correspond to the PL signal shown in Figure 4.2.

cannot be neglected. Nonclassical statistics occurs at the position of the inner ring, where the exciton gas is already cold but still dense. Furthermore, for $T_b \sim 0.1\,K$ (not yet realized in an optical imaging experiment) numerical modelling with Equation 4.1-4.6 give well-developed Bose-Einstein statistics with $N_{E=0}^{max}(r \simeq r_{rg}) \gg 1$.

4.2 Kinetics of the Inner Ring

4.2.1 Introduction

In the regular steady state excitation scheme, where excitons are generated in a micron scale focused laser excitation spot, the inner ring forms around the excitation spot. It was discussed in section 4.1 in terms of the cooling of indirect excitons during their propagation away from the excitation spot [Butov et al., 2002; Ivanov et al., 2006]. In this section, we present studies of the spatially and spectrally resolved kinetics of the exciton inner ring [Hammack et al., 2009]. The results show that the exciton inner ring forms and reaches a steady state within the first few tens of nanoseconds of laser excitation, and also disappears within a few nanoseconds after the laser termination. The spatially-temporal behavior of the inner ring is modelled in terms of in-plane exciton transport and cooling towards the phonon bath (cryostat) temperature.

4.2.2 Experimental data and numerical simulations

The measurements were performed using time-resolved imaging with 4 ns time-resolution and 2 μm spatial resolution. See section 3.1 for details of the experimental apparatus. Excitons were photogenerated by a pulsed laser at 635 nm with pulse duration of 500 ns and edge sharpness of < 1 ns, operating with a period of 1 μs. The period and duty cycle were chosen such that the photoluminescence pattern of indirect excitons was able to reach equilibrium during the laser excitation and to allow for complete decay of the PL of indirect excitons between laser pulses. The laser is focused to a 10 μm full width half

maximum (FWHM) excitation spot on the CQW sample. The excitation density P_{ex} was chosen to be below that at which the external ring appears in the emission pattern [Butov et al., 2002]. The spectral diffraction and time-gated imaging combined allow the direct visualization of the evolution of the indirect exciton PL intensity and energy as a function of delay time t [see Figure 4.4 (a)-(c) for the laser onset and Figure 4.4 (d)-(f) for the laser termination]. Experiments were performed at the applied gate voltage 1.2 V, peak excitation power 150 μW, and bath temperature 1.4 K.

The CQW structure used in these experiments is the same as in section 4.1.

Figure 4.4 (a)-(c) shows the emergence in time of an arrow shaped profile of the indirect exciton PL signal plotted in the energy − in-plane y axis, $E - y$, coordinates. The central bright stripe corresponds to the bulk n^+ GaAs emission. The n^+ GaAs layers are separated 200 nm from the CQW and their emission line spreads down to about 1.48 eV. Its spatial profile essentially corresponds to the laser excitation profile. The emission of indirect excitons is observed at the sides of this stripe beyond the excitation spot, due to the exciton transport. The emission energy drops with increasing distance from the origin r (see Figure 4.4). The drop in energy with increasing r corresponds to a decrease in density. At early times, when the indirect exciton signal is small, the bulk emission, consisting of the central bright stripe, dominates [see Figure 4.4 (a)]. After sufficient time, the exciton inner ring becomes apparent by the presence of a dip in the PL of indirect excitons within the region of laser excitation at the center of the exciton cloud. It is worth noting that the decrease in the exciton PL does not correspond to a dip in the exciton density, which has its maximum at the center of the laser excitation spot (see Figure 4.4).

The kinetics presented in Figure 4.5 (a) and (c) show the total spectrally integrated PL intensity of indirect excitons taken from a series of time-gated spectrally resolved images. The data shows that the inner ring forms and reaches a steady state within the first few tens of ns of the laser excitation pulse. Both the spatial and temporal character of the experimental data is in agreement with simulations using a kinetic model for the indirect exciton transport, cooling

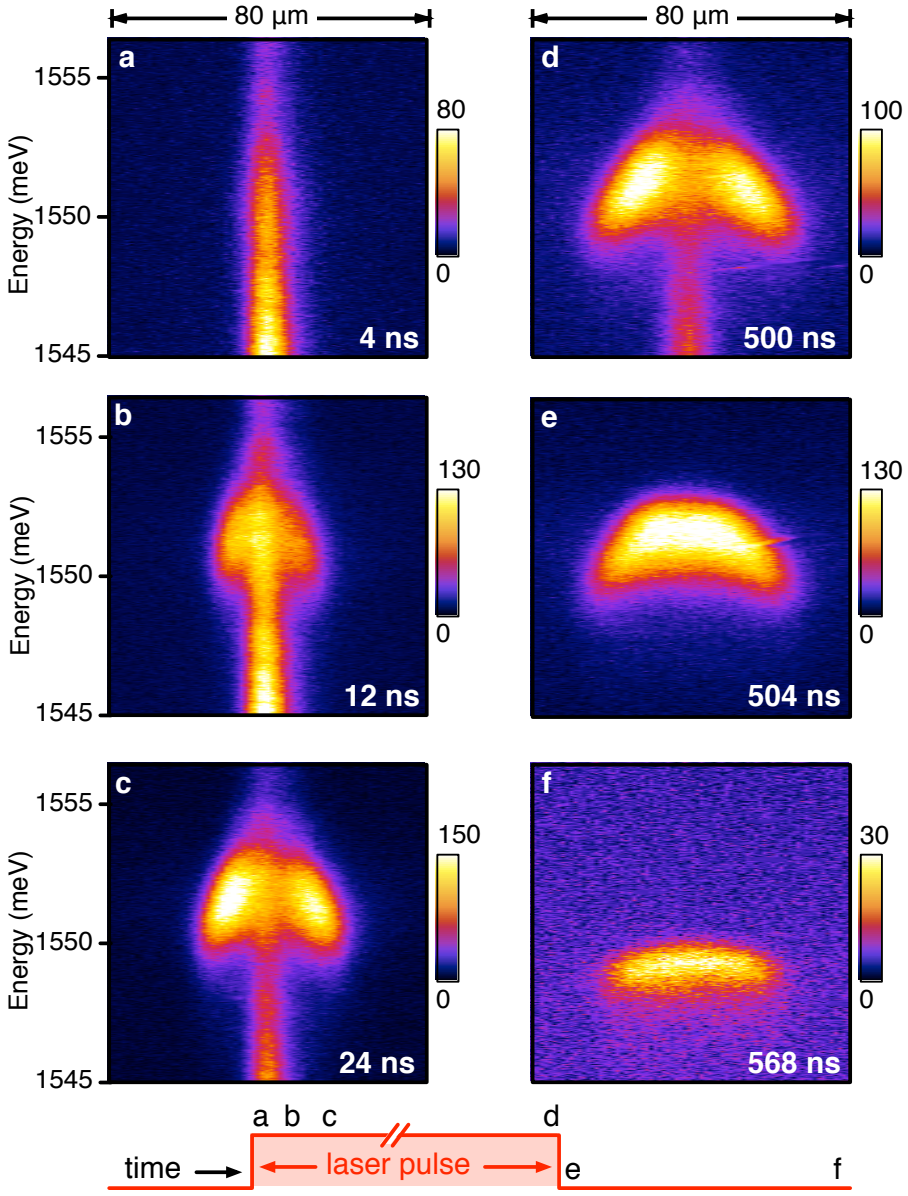

Figure 4.4: The $E - y$ images showing the exciton energy versus radius during the time evolution of the exciton inner ring following the onset and termination of the rectangular laser pulse. Time $t = 0$ ns corresponds to the onset of the laser pulse of the duration $\tau_{\text{pulse}} = 500$ ns. Each image is integrated over a time window of $\delta t = 4$ ns ending at the times (a)-(c) $t = 4$ ns, 12 ns, and 24 ns after the start of the laser pulse, and (d)-(f) $t - \tau_{\text{pulse}} = 0$ ns, 4 ns, and 68 ns after its termination. The laser is focused to a 10 μm full width half maximum (FWHM) excitation spot on the CQW sample.

and optical decay [see Figure 4.5 (a) *vs.* Figure 4.5 (b), and Figure 4.5 (c) *vs.* Figure 4.5 (d)]. The model is detailed in subsection 4.2.3.

These results demonstrate that within few tens of ns the excitons are able to propagate tens of microns away from the generation region. The large-scale transport is indicative that excitons are capable to screen effectively the disorder potential intrinsic to the quantum wells, leading to enhanced drift and diffusion [Ivanov, 2002]. This is consistent with the exciton diffusion coefficient D_x evaluated with the thermionic model and plotted in Figure 4.8 (d): An increase of D_x at a given radius r with increasing time (increasing exciton density) and a decrease of D_x at a given time t with increasing radius (decreasing density) are seen. The underlying physics is further illustrated in Figure 4.8, where numerical simulations of $T = T(t)$, $D_x = D_x(t)$, $n_x = n_x(t)$, and the optical lifetime of indirect excitons, $\tau_{opt} = \tau_{opt}(t)$, are plotted for the onset of the laser excitation.

Upon termination of the laser pulse [see Figure 4.4 (d)-(f)], an abrupt increase of the PL intensity is detected at the laser excitation spot [see Figure 4.6 (a), (c), and (e)]. After the laser switches off, the optically dark, high-energy excitons outside the light cone relax to the radiative zone, leading to the observed *PL-jump*. Experiments performed without spatial resolution have already revealed the PL-jump [Butov et al., 2001]. However, the results of the time-resolved imaging experiments presented here clarify that the PL-jump is observed predominantly within the laser excitation spot, where indirect excitons are heated by the laser. Within 4 ns, the time resolution of the current experiments, the excitons cool down to the lattice temperature $T_b = 1.4$ K. The characteristic cooling (thermalization) time, as calculated with the model described in Section III, is $\tau_{th} \simeq 0.2$ ns [see Figure 4.8 (a)]. The contrast of the PL-jump is defined as $(I_{max} - I_{laser\,on})/I_{laser\,on}$ with $I_{max} = I_{max}(r)$ and $I_{laser\,on} = I_{laser\,on}(r)$ the maximum PL intensity after the laser pulse termination and the steady-state PL-intensity in the presence of the laser pulse, respectively. The measured contrast of the PL-jump against the radial distance r is plotted in Figure 4.6 (c). Averaging the numerical simulations [see inset in 3 (d)] over the 4 ns integration window to match the experimental conditions leads to the PL-jump contrast shown in Figure 4.6 (d),

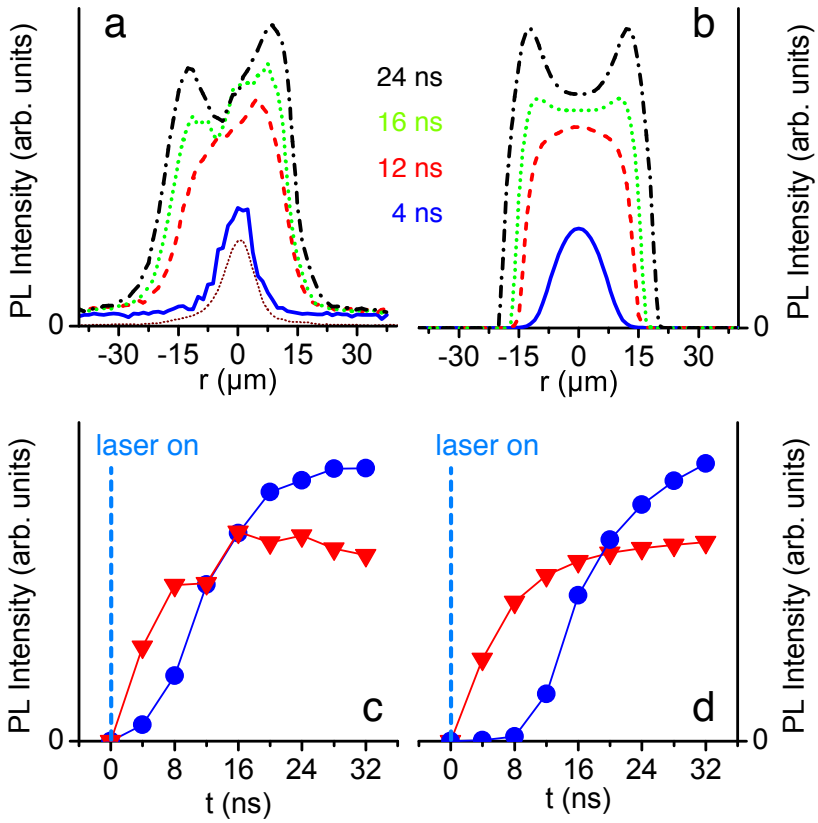

Figure 4.5: Kinetics of the indirect exciton PL profile after the laser excitation onset. The measured (a) and calculated (b) cross-sections of the indirect exciton PL across the diameter of the inner exciton ring as a function of time. The measured (c) and calculated (d) indirect exciton PL intensity at the center of the laser excitation spot (red ▼) and at the inner ring radius $r = r_{\text{ring}} \simeq 12\,\mu$m (blue ●) where the PL maximum signal occurs, as a function of time. The time integration window $\delta t = 4$ ns for each profile (a), (b) and each point (c), (d). The times $t = 0$ ns and $t = 500$ ns refer to the onset and termination of the rectangular laser excitation pulse. The laser excitation profile is shown by the thin dotted line in (a).

in agreement with the experiment [see Figure 4.6 (c) and (e) *vs*. Figure 4.6 (d) and (f)].

The monotonic decrease of the PL-jump with increasing radius [see Figure 4.6 (c)-(d)] demonstrates that the effective exciton temperature T during the laser excitation lowers with increasing r. This is consistent with the model we use: The numerical simulations of the exciton temperature profile, plotted in the inset of Figure 4.9 (a) for two time delays, 0 ns and 4 ns after the termination of the laser pulse, are in agreement with the spatial dependence of the PL-jump shown in Figure 4.6. Both the experimental data and calculations demonstrate that the exciton cooling time to the lattice temperature is much shorter than the exciton lifetime $\tau_{\rm opt} \simeq 50\,$ns.

4.2.3 Kinetic model

There are two main additional features in our present numerical simulations compared to those reported earlier section 4.1 in order to model a steady-state inner PL ring: (i) the high-resolution numerical simulations with Equation 4.1-Equation 4.3 are performed in a space-time domain instead of for steady state, and (ii) in order to mimic more closely the experiment, we model the source term $\Lambda_{\rm x}$ of indirect excitons (see the r.h.s. of Equation 4.1) by assuming a generation of incoming indirect excitons, as secondary particles, from laser-induced photocarriers.

In order to express $\Lambda_{\rm x}$ via the generation rate $\Lambda^{(0)}$ of free electron - hole pairs, which are photoexcited in the cladding AlGaAs layers and captured by the GaAs CQW structure, we implement the quantum mass action law (QMAL). According to the QMAL, a total number of electron-hole pairs is distributed among the bound (exciton) and unbound states. For quasi-2D indirect excitons, the QMAL reads as [Reinholz, 2002; Mouchliadis et al., 2007]

$$n_{\rm x} = -\frac{2M_{\rm x}k_{\rm B}T}{\pi\hbar^2}\ln\left[1 - e^{\epsilon_{\rm x}/(k_{\rm B}T)}\left(e^{T^{\rm e}_{\rm dB}/T} - 1\right)\left(e^{T^{\rm h}_{\rm dB}/T} - 1\right)\right], \tag{4.8}$$

where $\epsilon_{\rm x}$ is the (indirect) exciton binding energy, and the electron (hole) quantum

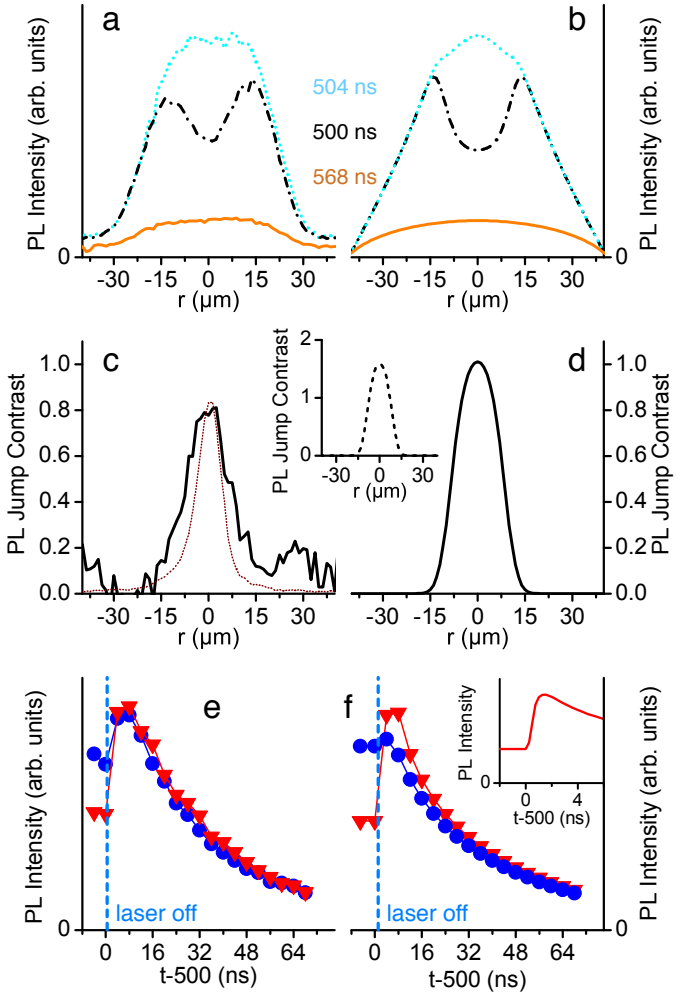

Figure 4.6: Kinetics of the indirect exciton PL profile during the laser excitation termination. The measured (a) and calculated with Equation 4.1-4.3 (b) spatial profiles of the PL signal from indirect excitons across the inner ring at the times $t = 500$ ns (dash-dotted line), 504 ns (dotted line), and 568 ns (solid line). The times $t = 0$ ns and $t = 500$ ns refer to the onset and termination of the rectangular laser excitation pulse. The measured (c) and evaluated numerically (d) contrast of the PL-jump $(I_{max} - I_{laser\,on})/I_{laser\,on}$ against the radial coordinate. The laser excitation profile is shown by the dotted line in (c). The measured (e) and calculated (f) PL intensity at the center of the laser excitation spot (red ▼) and at the radial distance where the PL maximum intensity occurs, $r = 12\,\mu$m, (blue ●) as a function of time. Insets: The contrast of the PL-jump (d) and the PL-jump at the center of excitation (f), evaluated with Equation 4.1-4.3 without time integration to match 4 ns experimental resolution. Apart from the insets, each calculated curve is smoothed by the device resolution function with the time integration window $\delta t = 4$ ns to match the experimental conditions.

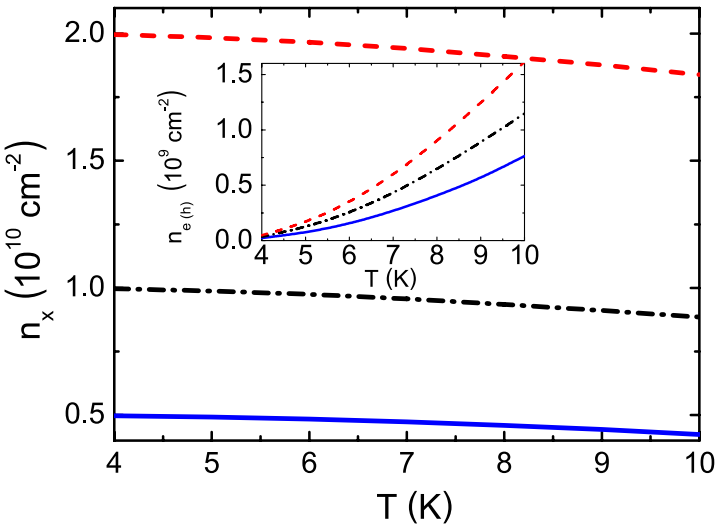

Figure 4.7: Exciton and electron (hole) concentrations, n_x and $n_e = n_h$, as a function of temperature, evaluated by using the quantum mass action law: $n_x + n_{e(h)} = 2 \times 10^{10}\,\mathrm{cm}^{-2}$ (dashed lines), $10^{10}\,\mathrm{cm}^{-2}$ (dash-dotted lines), and $0.5 \times 10^{10}\,\mathrm{cm}^{-2}$ (solid lines).

degeneracy temperature is given by $k_B T_{dB}^{e(h)} = \left[(\pi\hbar^2)/m_{e(h)}\right] n_{e(h)}$ with $m_{e(h)}$ and $n_{e(h)}$ the electron (hole) mass and concentration, respectively. Equation 4.8 characterizes a quasi-equilibrium balance between n_x and $n_e = n_h$. A typical time τ_{QMAL} needed to quasi-equilibrate the system of electrons, holes and indirect excitons is comparable to that of binding of photoexcited electrons and holes in excitons. The latter one is about $10 - 30\,\mathrm{ps}$ for $n_x \simeq 10^{10}\,\mathrm{cm}^{-2}$ and helium temperatures [Damen et al., 1990; Strobel et al., 1991; Blom et al., 1993; Gulia et al., 1997; Szczytko et al., 2004]. Because τ_{QMAL} is much less than the characteristic times of the thermalization and transport processes, $\tau_{th} \sim 0.1\,\mathrm{ns}$ and $\tau_{diff} \sim 1\,\mathrm{ns}$, the use of the QMAL is justified. For the case $T_{dB}^{e(h)} \ll T$, relevant to the experiment, Equation 4.8 yields:

$$\Lambda_x = \Lambda^{(0)} \frac{4M_x T_{dB}^{1/2}}{(m_e m_h T)^{1/2} e^{-\epsilon_x/(2k_B T)} + 4M_x T_{dB}^{1/2}}\,. \tag{4.9}$$

Note that in Equation 4.9 the degeneracy temperature T_{dB} is proportional to the accumulated density of indirect excitons, $n_x = n_x(r,t)$. According to numerical

evaluations of Equation 4.9 adapted to the experimental conditions, apart from the first few hundred picoseconds after the onset of the laser excitation, when $T \gtrsim 10\,\mathrm{K}$ and $n_\mathrm{x} \lesssim 10^9\,\mathrm{cm}^{-2}$, one has $n_\mathrm{x} \gg n_\mathrm{e(h)}$, see Figure 4.7, and $\Lambda_\mathrm{x} \simeq \Lambda^{(0)}$. Formally, this is because in the denominator on the r.h.s. of Equation 4.9 the term $(m_\mathrm{e} m_\mathrm{h} T)^{1/2} e^{-\epsilon_\mathrm{x}/(2k_\mathrm{B}T)}$ is much less than $4M_\mathrm{x}T_\mathrm{dB}^{1/2}$. In this case, injected electron-hole pairs very effectively transfer to the exciton system.

The observed inner PL ring is nearly radially symmetric in space, when taking the center of the excitation spot as the origin, see Figure 4.1. Thus in numerical simulations with Equation 4.1-Equation 4.3, a polar coordinate system is used and the condition invoked that none of the quantities modelled have any angular dependence. According to the spatial profile of the laser pulse, we assume that the generation rate $\Lambda^{(0)}$ is given by the Gaussian:

$$\Lambda^{(0)} = \Lambda^{(0)}(r,t) = \Lambda^{(0)}(r=0,t)\, e^{-r^2/r_0^2}, \tag{4.10}$$

with r_0 the radius of the excitation spot [$r_0 = \mathrm{FWHM}/(2\sqrt{\ln 2}) = 5.8\,\mu\mathrm{m}$]. The temporal shape of the rectangular laser pulse with the Gaussian edges is modelled by $\Lambda^{(0)}(r=0,t)$, where $\Lambda^{(0)}(r=0,t) = \tilde{\Lambda}^{(0)} \exp[-\sigma(t-t_0)^2]$ for $t \leq t_0 = 0.6\,\mathrm{ns}$, $\tilde{\Lambda}^{(0)}$ for $t_0 \leq t \leq \tau_\mathrm{pulse} = 500\,\mathrm{ns}$, and $\tilde{\Lambda}^{(0)} \exp[-\sigma(t-\tau_\mathrm{pulse})^2]$ for $t \geq \tau_\mathrm{pulse}$, and $\sigma = 15.3\,\mathrm{ns}^{-2}$.

In order to clarify further the underlying physics of the inner PL ring, in Figure 4.8 and Figure 4.9 we plot $T = T(t)$, $n_\mathrm{x} = n_\mathrm{x}(t)$, $\tau_\mathrm{opt} = \tau_\mathrm{opt}(t)$, and $D_\mathrm{x} = D_\mathrm{x}(t)$, modelled for the onset and termination edges of the laser excitation pulse, respectively. The shown dynamics refer to the center of the excitation spot (solid lines), the radial distance $r = r_\mathrm{ring}$ where a maximum PL signal occurs (dashed lines), $r = r_\mathrm{ring}/2$ (dotted lines), and $r = 3r_\mathrm{ring}/2$ (dash-dotted lines).

For the onset of the laser excitation, Figure 4.8 (a) and (b) illustrate the thermalization kinetics of indirect excitons and gradual building up of the density, respectively. The monotonic decrease of τ_opt with time is due to the cooling of indirect excitons [see Figure 4.8 (c)]. A steady-state value of the optical lifetime decreases with increasing r, because the laser induced heating of the exciton system decreases with the radial distance from the laser spot center. The initial

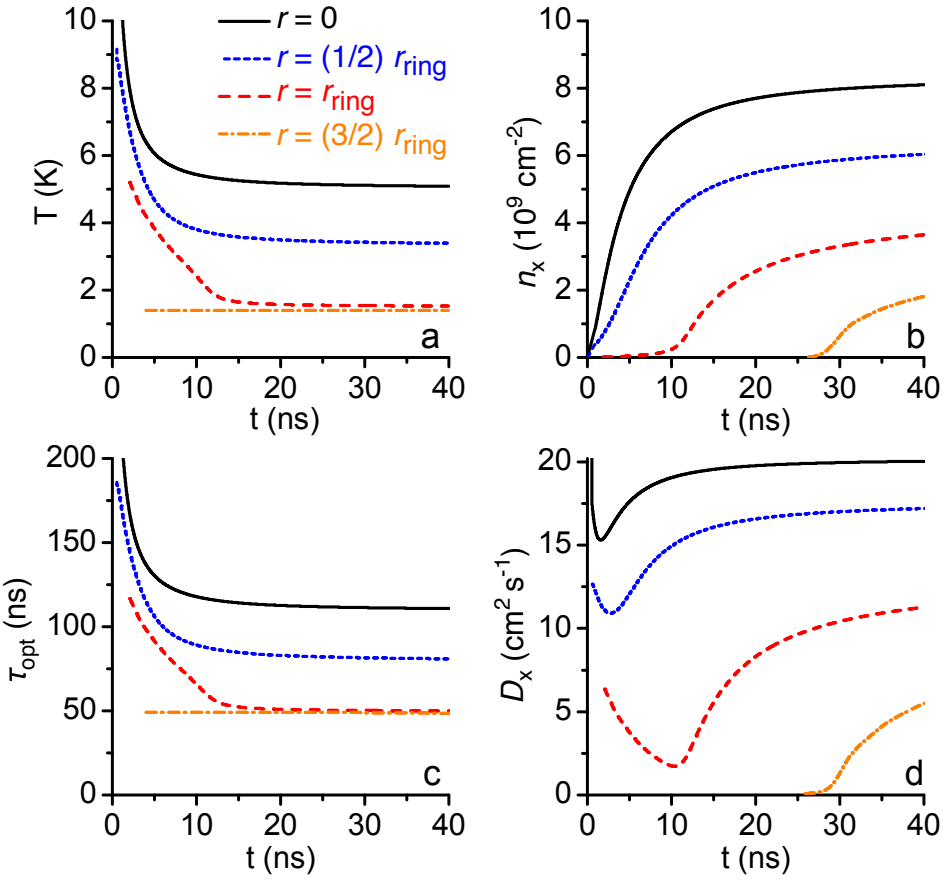

Figure 4.8: Modeling of the transient dynamics of the exciton temperature T (a), density n_x (b), optical lifetime τ_{opt} (c), and in-plane diffusion coefficient D_x (d) for the onset of the laser excitation. The radial coordinate is $r = 0$ (solid line), $r_{ring}/2$ (dotted line), r_{ring} (dashed line), and $3r_{ring}/2$ (dash-dotted line).

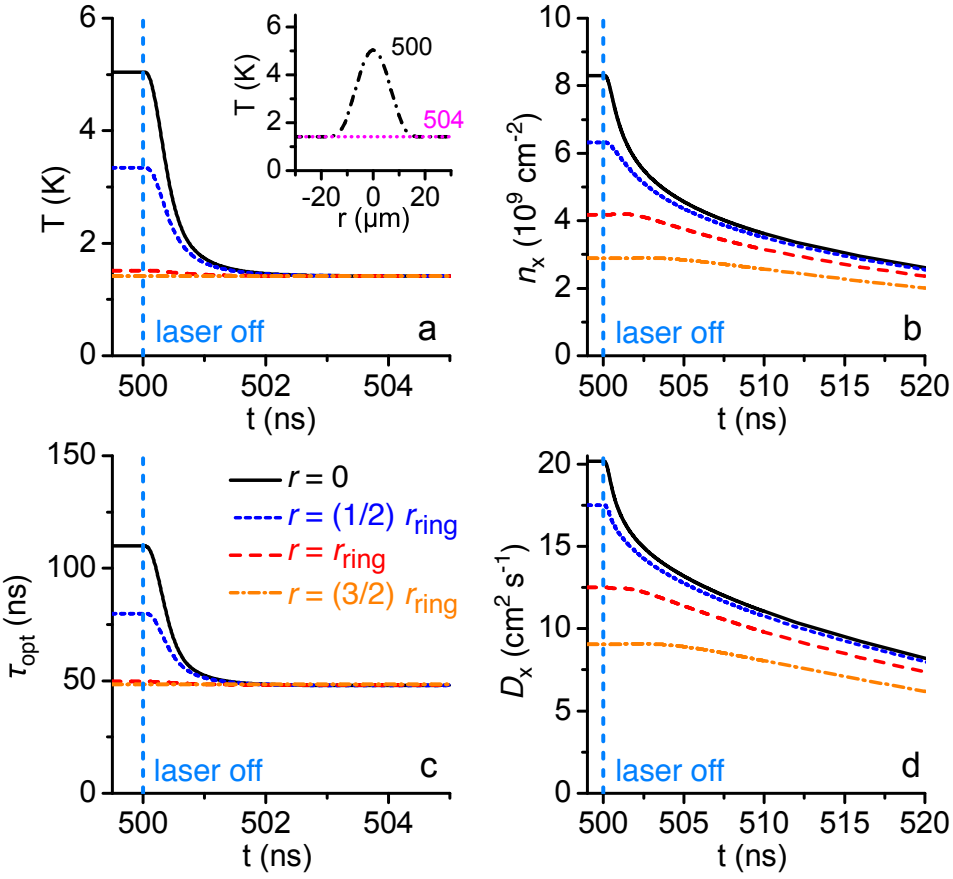

Figure 4.9: Modelling of the transient dynamics of the exciton temperature T (a), density n_x (b), optical lifetime τ_{opt} (c), and in-plane diffusion coefficient D_x (d) for the termination of the laser excitation. The radial coordinate is $r = 0$ (solid line), $r_{ring}/2$ (dotted line), r_{ring} (dashed line), and $3r_{ring}/2$ (dash-dotted line). Inset: The calculated spatial profile of the exciton temperature, $T = T(r)$, for $t = 500$ ns (solid line) and $t = 504$ ns (dotted line).

rapid decrease of D_x [see Figure 4.8 (d)] originates from the thermalization of the exciton system: Cold excitons cannot overcome the in-plane disorder potential and become localized. A further increase of the diffusion coefficient after the thermalization transient is due to the screening effect which develops with increasing n_x.

For the termination edge of the laser pulse, the decay dynamics shown in Figure 4.9 are dominated by the two characteristic times, thermalization time τ_{th} and optical decay time $\tau_{opt} \gg \tau_{th}$. Within first $1-2$ ns the complete thermalization occurs [see Figure 4.9 (a)], and the system of indirect excitons decays with $\tau_{opt} = \tau_{opt}(T = T_b) \simeq 50$ ns [see Figure 4.9 (b) and (c)]. The gradual decrease of D_x at delay times much larger than τ_{th} [see Figure 4.9 (d)] is due to the relaxation of the screening effect with decreasing density of indirect excitons.

4.2.4 Discussion

Numerical simulations with Equation 4.1-Equation 4.3 quantitatively reproduce the experimental data [see in Figure 4.5 and Figure 4.5 experiment *vs.* modelling] for the following control parameters: $U_0 = 0.7$ meV, $D_x^{(0)} = 30\,\mathrm{cm}^2/\mathrm{s}$, $\tilde{\Lambda}^{(0)} = 2 \times 10^9\,\mathrm{cm}^{-2}\mathrm{ns}^{-1}$, and $E_{inc} = 12.9$ meV. Although we use four fitting parameters, the procedure is well justified: (i) The whole set of the experimental data, measured at various r and t, are modelled with the same values of the control parameters, and (ii) the fitting parameters influence different aspects of the transport and PL processes in a separate way, i.e., can be inferred independently. Table I lists the inferred values of the control parameters as well as the known values, the basic parameters, and the parameters of the model.

The model includes the nonclassical, quantum-statistical effects in the description of the transport, thermalization and optical decay of indirect excitons: Equation 4.1-4.6 and Equation 4.8-4.9 explicitly depends upon T_{dB}. However, the quantum corrections are rather minor, due to relatively weak laser excitations used in the experiment. The quantum effects are not required for the inner ring or the PL-jump formation. Both are classical phenomena associated with the exciton cooling when they travel away from the excitation spot (in the

Table 4.1: List of Parameters

Basic Parameters		Model Parameters	
M_x	$0.22\,m_0$	$D_x^{(0)}$	$30\,cm^2\,s^{-1}$
τ_{sc}	110 ns	U_0	0.7 meV
τ_R	20 ns	$\tilde{\Lambda}^{(0)}$	$2\times10^9\,cm^{-2}\,ns^{-1}$
v_s	$3.7\times10^5\,cm\,s^{-1}$	E_{inc}	12.9 meV
ρ	$5.3\,g\,cm^{-3}$	u_0	$1.6\times10^{-10}\,meV\,cm^2$
D_{dp}	8.8 eV		
T_b	1.4 K		
E_0	34.2 μeV		
E_γ	138 μeV		
L_z	8 nm		

case of the inner ring) or when the excitation pulse is terminated (in the case of the PL jump). However, the quantum degeneracy effects become essential for the dynamics and contrast of the inner PL ring and PL-jump, if smaller bath temperatures or higher excitation powers are used [Butov et al., 2001; Ivanov et al., 2006; Hammack et al., 2006a]. For instance, bosonic stimulation of exciton scattering can lead to the enhancement of the exciton scattering rate to the low-energy optically active states with increasing exciton concentration as described in Ref. [Butov et al., 2001].

Note that a ring in the emission pattern can form both in an exciton system [Butov et al., 2002; Ivanov et al., 2006] and in an electron-hole plasma (EHP) [Stern et al., 2008]. In both cases the requirements for the ring formation in the emission pattern include the long lifetime of the carriers, which allows transport over substantial distances, and cooling of the carriers during their transport away from the excitation spot, which leads to the increase of the emission intensity. However, the exciton system can be distinguished from EHP by the emission linewidth. For a neutral quasi-2D EHP, the emission linewidth should be about the sum of the electron and hole Fermi energies, $\Delta_{EHP} \simeq k_B T^e_{dB} + k_B T^h_{dB} = \pi\hbar^2 n_{e(h)}(1/m_e + 1/m_h)$, with $n_e = n_h$ the density of electrons and holes in EHP [Butov et al., 1991]. The smallest density for EHP is determined by the exciton Mott transition $n_M \sim 1/a_B^2$, which occurs due to the phase space filling and screening (a_B is the exciton Bohr radius) [Schmitt-Rink

et al., 1989]. For the CQW structures studied, $m_e \simeq 0.07\,m_0$ and $m_h \simeq 0.15\,m_0$ [Lozovik et al., 2002], the Bohr radius of the indirect excitons $a_B \simeq 20$ nm [Dignam & Sipe, 1991] and $n_M \sim 1/a_B^2 \sim 2\times10^{11}$ cm^{-2}, so that the smallest linewidth for the EHP is $\Delta_{EHP}^{min} \simeq \pi\hbar^2 n_M(1/m_e+1/m_e) \sim 10$ meV. In contrast, the linewidth of exciton emission can be well below this value. It is determined by the homogeneous and inhomogeneous broadening and is typically below 2 meV in the CQW structures for the investigated range of densities [High et al., 2009b]. The small emission linewidth $\lesssim 2$ meV, which is characteristic for the inner ring reported in this dissertation and in the literature[Butov et al., 2002; Ivanov et al., 2006; Stern et al., 2008; Hammack et al., 2009], indicates that in all these experiments the inner PL ring forms in an exciton system rather than in EHP.

4.3 Summary

In summary, we studied steady state and kinetic character of the inner ring in the exciton emission pattern. The formation time of the inner ring following the onset of the laser excitation is found to be about 30 ns. The inner ring was also found to disappear within 4 ns after the laser termination. The latter process is accompanied by a jump in the PL intensity. The spatial dependence of the PL-jump indicates that the excitons outside of the region of laser excitation, including the inner ring region, are efficiently cooled to the lattice temperature even during the laser excitation. The ring formation and disappearance are explained in terms of exciton transport and cooling.

4.4 Acknowledgements

The text of chapter 4, in part, is a reprint of the material as it appears in AL Ivanov, LE Smallwood, AT Hammack, Sen Yang, LV Butov, & AC Gossard, *Origin of the inner ring in photoluminescence patterns of quantum well excitons*, Europhys Lett, **73**, 920 © 2006 European Physical Society, where the dissertation author was the first experimental author. The co-authors in this publication

directed, supervised, and co-worked on the research with forms the basis of this chapter.

The text of chapter 4, in part, is a reprint of the material as it appears in AT Hammack, LV Butov, J Wilkes, L Mouchliadis, EA Muljarov, AL Ivanov, & AC Gossard, *Kinetics of the inner ring in the exciton emission pattern in coupled GaAs quantum wells*, Phys Rev B **80**, 155331, © 2007 The American Physical Society, where the dissertation author was the first author. The co-authors in this publication directed, supervised, and co-worked on the research with forms the basis of this chapter.

5 Optical Control

5.1 An optically induced exciton trap

5.1.1 Introduction

Lasers enable a precise and non-invasive application of force while also providing high speed control of the trapping field. This allows *in-situ* trapping and control for a rich variety of small neutral particles. Since their origin three decades ago, laser based traps have been key devices in the advancement of atomic physics and biophysics, for reviews see [Chu, 1998; Cohen-Tannoudji, 1998; Phillips, 1998; Ashkin, 2000].

In biology, the applications of optical dipole traps, also known as optical tweezers, enable direct *in-vivo* manipulation of viruses, cells, and even individual organelles within the cells. The use of optical tweezers has also enabled probing of the mechanical properties of DNA and the forces applied by various molecular motors found in cells [Ashkin, 2000].

In atomic physics, the use of the Doppler cooling technique [Hänsch & Schawlow, 1975] by sets of counter propagating lasers is employed to form an "optical molasses" containing atoms viscously confined at microkelvin temperatures. The introduction of optical tweezers to this molasses enabled the first 3D stable trap for atoms by capturing them from the surrounding molasses. Following this initial trapping of atoms, much work was devoted to the creation of larger volume magneto-optical traps (MOT) to enhance the achievable densities of trapped atoms [Chu, 1998; Cohen-Tannoudji, 1998; Phillips, 1998; Ashkin, 2000]. It was specifically these MOTs that led to the first realizations

of Bose-Einstein condensation (BEC) in atoms [Anderson et al., 1995; Bradley et al., 1995; Davis et al., 1995]. Since this initial realization of BEC, interest has returned again to optical traps, which can be used to study magnetic effects on BEC, such as Feshbach resonances, without the complexity added by disrupting the magnetic field used in MOTs [Chu, 1998; Cohen-Tannoudji, 1998; Phillips, 1998; Ashkin, 2000]. The possibility of patterning and controlling the potential profile by laser excitation is also effectively employed in studies of atom BEC in optical lattices [Greiner et al., 2002].

In this section, we propose and demonstrate laser induced trapping for a new system - a gas of excitons in coupled quantum wells (CQW) [Hammack et al., 2006b]. Since the quantum degeneracy temperature scales inversely with the mass, quantum exciton gases can be achieved at temperatures of about 1 K [Keldysh & Kozlov, 1968], several orders of magnitude higher than quantum atom gases [Cornell & Wieman, 2002; Ketterle, 2002]. Indeed, the transition from a classical to quantum gas occurs when bosons are cooled to the point where the thermal de Broglie wavelength $\lambda_{\mathrm{dB}} = \sqrt{2\pi\hbar^2/(mk_BT)}$ is comparable to the interparticle separation (for instance, BEC takes place when $n\lambda_{\mathrm{dB}}^3 = 2.612$ in 3D systems) and the transition temperature for excitons in GaAs/AlGaAs QWs reaches a value of $T_{\mathrm{dB}} = 2\pi\hbar^2 n_{2\mathrm{d}}/(mgk_B) \approx 3\,\mathrm{K}$ for the exciton density per spin state $n_{2\mathrm{d}}/g = 10^{10}\,\mathrm{cm}^{-2}$ (the exciton spin degeneracy $g = 4$ and the exciton mass $m = 0.22m_0$ for GaAs/AlGaAs QWs [Butov et al., 2004], where m_0 is the free electron mass). Because of their long lifetime and high cooling rate, indirect excitons in a CQW (Figure 5.1a) form a system where a cold and dense exciton gas can be created, with temperatures well below 1 K and densities above $10^{10}\,\mathrm{cm}^{-2}$ [Butov et al., 2004]. Therefore, we chose indirect excitons for development of a method to trap cold excitons with laser light. This technique opens a pathway towards high speed control of quantum gases of bosons in semiconductors—quantum exciton gases.

The possibility of exciton confinement and manipulation in potential traps attracted considerable interest in earlier studies. Pioneered by the electron-hole liquid confinement in the strain-induced traps [Wolfe et al., 1975], exci-

ton confinement has been implemented in various traps: strain-induced traps [Trauernicht et al., 1983; Kash et al., 1988], traps created by laser-induced local interdiffusion [Brunner et al., 1992], magnetic traps [Christianen et al., 1998], and electrostatic traps [Zimmermann et al., 1997; Huber et al., 1998; Hammack et al., 2006a].

The principle underlying the new method of laser induced exciton trapping is described below. The CQW geometry is engineered so that the interaction between excitons is repulsive: Indirect excitons, formed from electrons and holes that are confined to different QWs by a potential barrier, behave as dipoles oriented perpendicular to the plane, and an increasing exciton density causes an increase of the interaction energy [Yoshioka & MacDonald, 1990; Zhu et al., 1995; Ivanov, 2002]. The repulsive character of the interaction is evidenced in experiment as a positive and monotonic line shift with increasing density [Butov et al., 2004]. Due to the repulsive interaction, a ring-shaped laser spot should form a potential trap with the energy minimum at the ring center. Similarly to all optical traps, an important advantage of the laser induced exciton trapping is the possibility of controlling the trap *in-situ* by varying the laser intensity in space and time. Moreover, the excitons at the trap center are cold since they are far from the hot laser excitation ring. The long lifetimes of the indirect excitons allow them to travel to the trap center, due to their drift and diffusion, before optical recombination. This leads to accumulation of a cold and dense exciton gas at the trap center. The implementation of this idea is described below.

5.1.2 Experimental methods

The spatial x-y (see Figure 5.1c-e) and E-y (see Figure 5.1b) images are collected by the means outlined in section 3.1. Our investigations determined that a laser excitation ring with a diameter of 30 μm and a ring thickness following a Gaussian profile of FWHM = $2\sigma \simeq 7$ μm provided the optimal conditions for our CQW sample. The ring shaped cw laser excitation was performed by Nd:YVO_4 laser at 532 nm, or HeNe laser at 633 nm, or Ti:Sapphire laser tuned to the direct exciton resonance of 788 nm. Spatial and spectral features were es-

sentially similar for all excitation wavelengths investigated. In the experiments with excitation above the AlGaAs barrier (λ = 532 or 633 nm), photoexcited unbalanced charges and the external ring are created, while in the experiments at nearly resonant excitation (λ = 788 nm), no photoexcited unbalanced charges or external ring are created [Butov et al., 2004]. Comparison of these two experiments has shown that the charge imbalance and external ring make no noticeable effect on the exciton trapping. All experimental data presented here are from a set of 532 nm excitation ring data taken with excitation powers $P_{\rm ex}$ in the range 1-1000 μW and with gate voltage $V_{\rm g}$ = 1.4 V. The CQW structure investigated is grown by molecular beam epitaxy and contains two 8 nm GaAs QWs separated by a 4 nm $Al_{0.33}Ga_{0.67}As$ barrier (see section 3.2.

5.1.3 Experimental data and numerical simulations

As can be seen in Figure 5.1c-e and Figure 5.2a, for low excitation powers the PL profile follows the laser excitation ring; however, with increasing excitation power a spatial PL peak emerges at the center of the laser excitation ring, indicating the accumulation of a cold and dense exciton gas. The exciton degeneracy at the trap center $N_{E=0} = \exp(T_0/T) - 1$, where $T_0 = 2\pi\hbar^2 n_{\rm 2d}/(mgk_B)$ [Ivanov et al., 1999], can be estimated from the exciton density and temperature. The exciton density $n_{\rm 2d} = \varepsilon\delta E/(4\pi e^2 d)$ is measured directly by the exciton energy shift δE, where d = 12 nm is the separation between the electron and hole layers for our samples and ε is the background dielectric constant [Yoshioka & MacDonald, 1990; Zhu et al., 1995; Ivanov, 2002] ($n_{\rm 2d} = 10^{10}\,{\rm cm}^{-2}$ for $\delta E \simeq 1.6$ meV). The exciton temperature at the trap center is essentially equal to the lattice temperature due to absence of heating sources at the trap center. The estimate shows that for the excitation $P_{\rm ex}$ = 1000 μW and temperature $T_{\rm b}$ = 1.4 K, see the experimental data in Figure 5.2, the exciton degeneracy at the trap center is $N_{E=0} \simeq 8$. The theoretical modeling presented below confirms this estimate.

Note that the exciton trapping by laser light is based on a different physical principle compared to the atom trapping by laser light. However, the two techniques lead to conceptually similar optical trapping of quantum gases—of

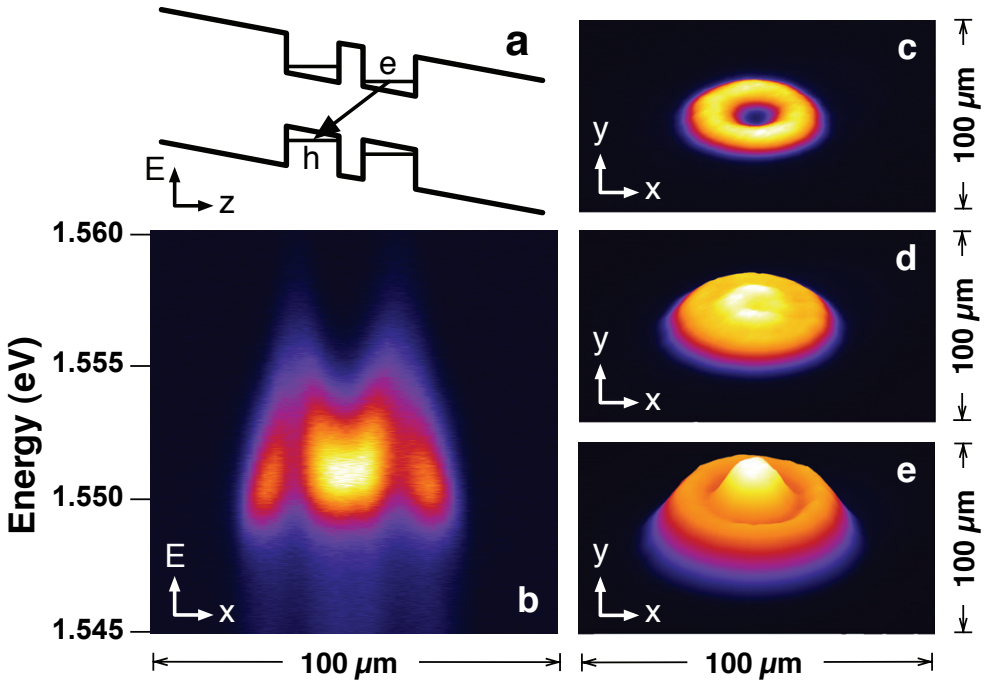

Figure 5.1: Images of laser-induced trapping of excitons. (a) Energy band diagram of the CQW structure; e, electron; h, hole. (b) Image of the PL signal in E-x coordinates. (c)-(e) Experimental x-y plots of the PL intensity from indirect excitons created by 532 nm cw laser excitation in a 30 μm diameter ring on the CQW sample. For (c)-(e) the excitation powers are $P_{\rm ex}$ = 10, 35, 100 μW and for (b) $P_{\rm ex}$ = 75 μW. Sample temperature $T_{\rm b}$ = 1.4 K.

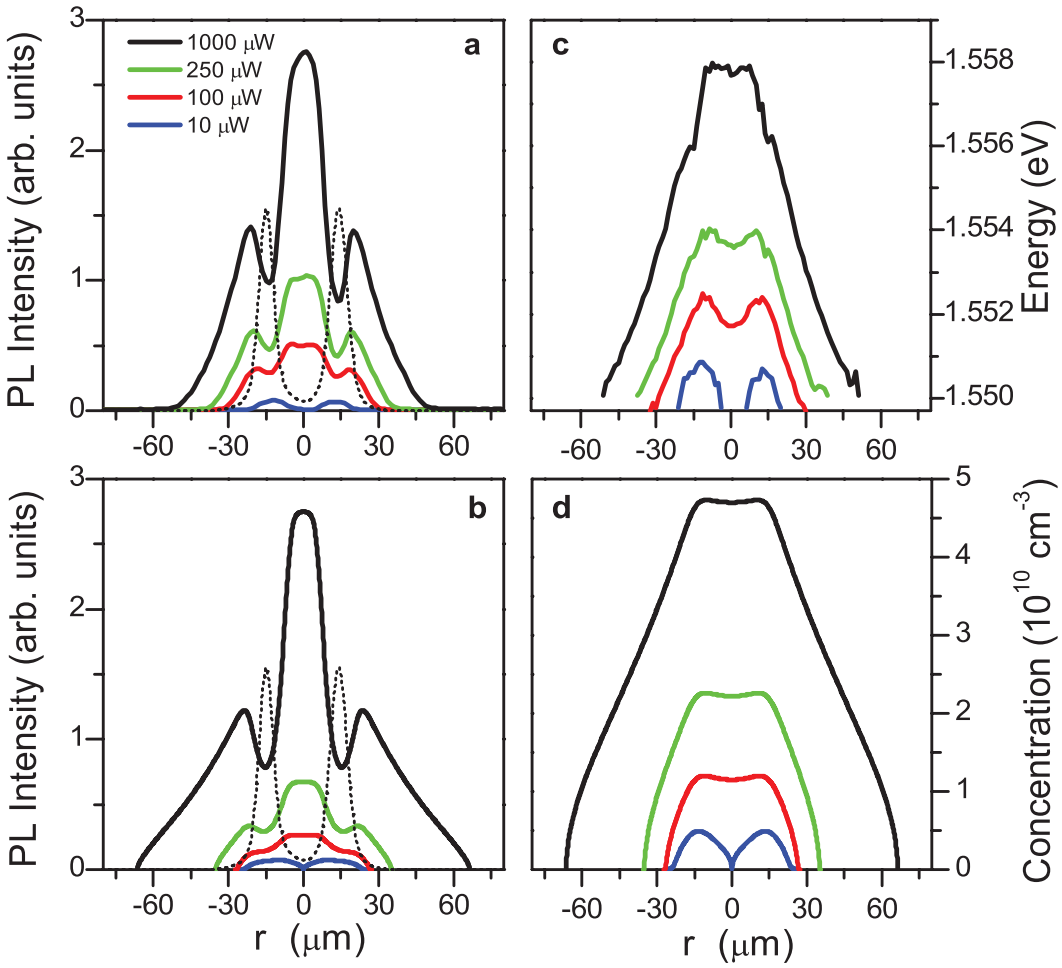

Figure 5.2: Spatial profiles of the PL intensity and energy for the excitons in the laser-induced trap. (a) Measured PL intensity, (b) calculated PL intensity, (c) measured energy position of the PL line, and (d) calculated exciton concentration against radius r for four optical excitation powers P_{ex}. The vertical axes of (c) and (d) cover the same range due to the relation $\delta E = 4\pi e^2 n_{2\mathrm{d}} d/\varepsilon$, where $d = 12\,\mathrm{nm}$ for our sample. The ring shaped profile of the laser excitation is shown by the thin dotted lines in (a) and (b). Sample temperature $T_{\mathrm{b}} = 1.4\,\mathrm{K}$.

excitons or atoms, respectively.

A parabolic energy trap is apparent in the interior of the excitation ring (Figure 5.1b and Figure 5.2c). The decrease in the indirect exciton PL at the location of the excitation ring (Figure 5.2a) is because the high-energy photo-generated excitons heat the exciton gas; this heating reduces the fraction of optically active excitons. As they drift and diffuse away from the excitation area, the excitons thermalize to the lattice temperature T_b and become optically active, leading to the moderately enhanced PL intensity directly external to the excitation ring. The strong enhancement of the PL at the excitation ring center, Figure 5.2a, is due to (1) the excitons' thermalization to the lattice temperature and (2) the accumulation of large numbers of excitons driven by dipole repulsion away from the higher density region towards the ring center.

The numerical simulations, based on a microscopic theoretical model, match the experimental results excellently (Figure 5.2b and d). Our approach to the transport, relaxation and PL dynamics of indirect excitons is formulated in terms of three coupled nonlinear equations: A quantum diffusion equation for the exciton density n_{2d}, a thermalization equation for the exciton temperature T, and an equation for the exciton optical lifetime τ_{opt} [Ivanov, 2002]. Calculation for the present experiment matches the technique outline in subsection 4.1.3 with the generation rate $\Lambda_x(r)$ chosen appropriately to match the laser excitation ring. A particular feature of the trap is that it is formed by the indirect excitons themselves: The trap potential is given in the mean-field approximation by $U_{trap} = \delta E = u_0 n_{2d} = 4\pi e^2 n_{2d} d/\varepsilon$, where u_0 is a positive scattering amplitude. Note that the trap confining potential is determined by the radial exciton density distribution and is essentially independent of other characteristics of indirect excitons such as their temperature, etc.. Quantum-statistical corrections [Ivanov, 2002] are included in the simulations.

The increase of the exciton gas temperature due to heating by photo-generated excitons at the excitation ring is evident in Figure 5.3a. A minor heating due to the exciton potential energy gradient can also be seen outside the excitation ring. The exciton transport towards the trap center due to drift and

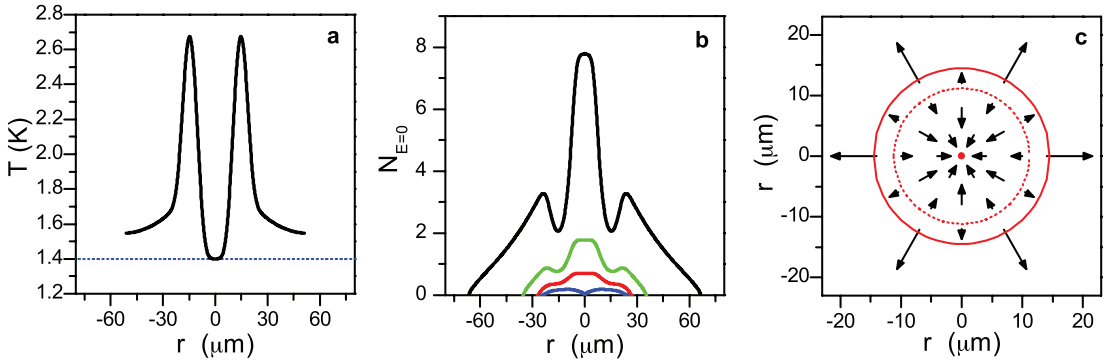

Figure 5.3: The calculated parameters of excitons in the laser-induced traps. (a) The radial dependence of the exciton temperature T for optical excitation power of 1000 μW (solid black) and the lattice temperature T_b = 1.4 K (dotted blue). (b) The occupation number $N_{E=0}$ for our samples against radius r for the same four optical excitation powers as in Figure 5.2. (c) Vector plot showing the calculated exciton velocities v for excitation power of 500 μW. The length of the outermost vectors is 1.3×10^6 cm/s. The dotted red line shows the maximum calculated exciton concentration and the solid red line shows the maximum of incident laser power used in calculation.

diffusion is illustrated in Figure 5.3c. Finally, the theoretical calculations confirm that in our experiments, which deal with the cryostat temperature T_b = 1.4 K, high nonclassical occupation numbers, $N_{E=0} \simeq 8$, build up at the trap center (Figure 5.3b).

5.2 Kinetics of the optically-induced exciton trap

5.2.1 Introduction

One of the most important characteristics of traps for Bose particles, which is crucial for the observation, probe, and control of these new quantum states, is the trap loading time. Apparently, studies of the degenerate gases in the traps require the fast loading of the gases to the trap, preferably on a timescale less than their lifetime in the trap. For the typical atomic optical traps, the loading times of the degenerate atomic gases are on the order of a few tens of seconds while their lifetimes in the trap are on the order of a few seconds [Lewandowski

et al., 2003; Streed et al., 2006].

Two of the typical trap types applied in the study of excitons — the electrostatic and the optically-induced traps — show promise of rapid and effective control of the excitons by varying in space and time the gate voltage pattern and the laser intensity pattern, respectively. Control of excitons by varying the electrostatic potential on a time scale much shorter than the exciton lifetime was recently demonstrated [Winbow et al., 2007]. This indicates the feasibility of studying excitons in controlled electrostatic traps. The current section presents the timescale of exciton control that is achievable in an optically-induced trap. The results demonstrate a rapid loading of the trap by cold excitons on a timescale less than the exciton lifetime and prove the feasibility of accumulating a spatially confined dense and cold exciton gas as well as the rapid *in situ* control of excitons in the traps.

5.2.2 Experimental methods and data

Figure 5.4a-d shows intensity profile of the indirect exciton emission in spatial coordinates as a function of delay time t. For a general description of the experimental methods, see section 3.1. For the study at hand, excitons were photogenerated using rectangular laser excitation pulses emitted by a pulsed semiconductor laser diode at 635 nm. The pulse duration was 500 ns, the edge sharpness < 1 ns, and the repetition frequency 1 MHz. The period and duty cycle were chosen to provide ample time for the exciton gas to reach equilibrium during the laser pulse and to allow complete decay of the indirect exciton photoluminescence (PL) between the pulses. The pulses were patterned into a laser excitation ring with a diameter of 30 μm and a ring thickness following a Gaussian profile of FWHM $= 2\sigma \simeq 10\,\mu$m using a shadow mask. This ring-shaped laser excitation created the in-plane spatial confinement of cold indirect excitons by exploiting their mean-field repulsive interaction, which forms the trapping profile (see section 5.1 and Hammack et al. [2006b]. For the studied CQW sample, $\varepsilon_b = 12.9$ and $d = 11.5$ nm [Butov et al., 2004].

The kinetics presented in Figure 5.5c-d demonstrate that the exciton pat-

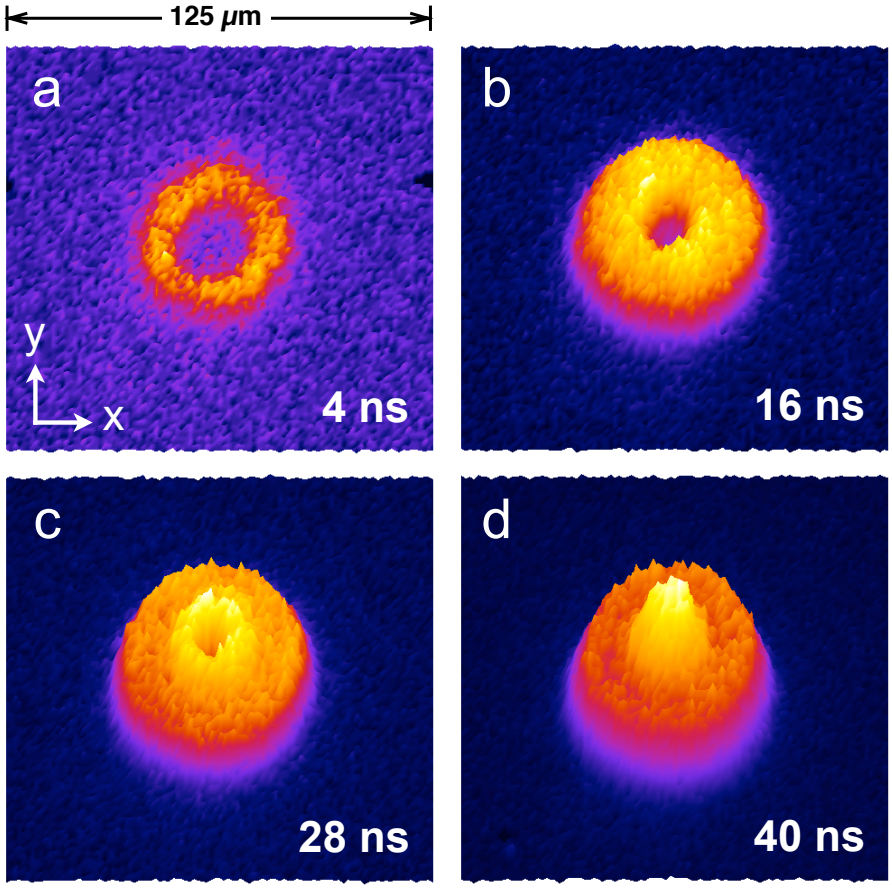

Figure 5.4: Time resolved images of optically-induced trapping of excitons collected by a photogated CCD. (a)-(d) x–y plots of the PL intensity from indirect excitons collected at delays of 4, 16, 28, and 40 ns relative to the start of 635 nm pulsed laser diode excitation in a 30 μm diameter ring on the CQW sample. The time-integration window for each image is 4 ns. Average excitation power $P_{\rm ex} = 75\,\mu$W. Bath temperature $T_{\rm b} = 1.4$ K. $V_{\rm g} = 1.2$ V.

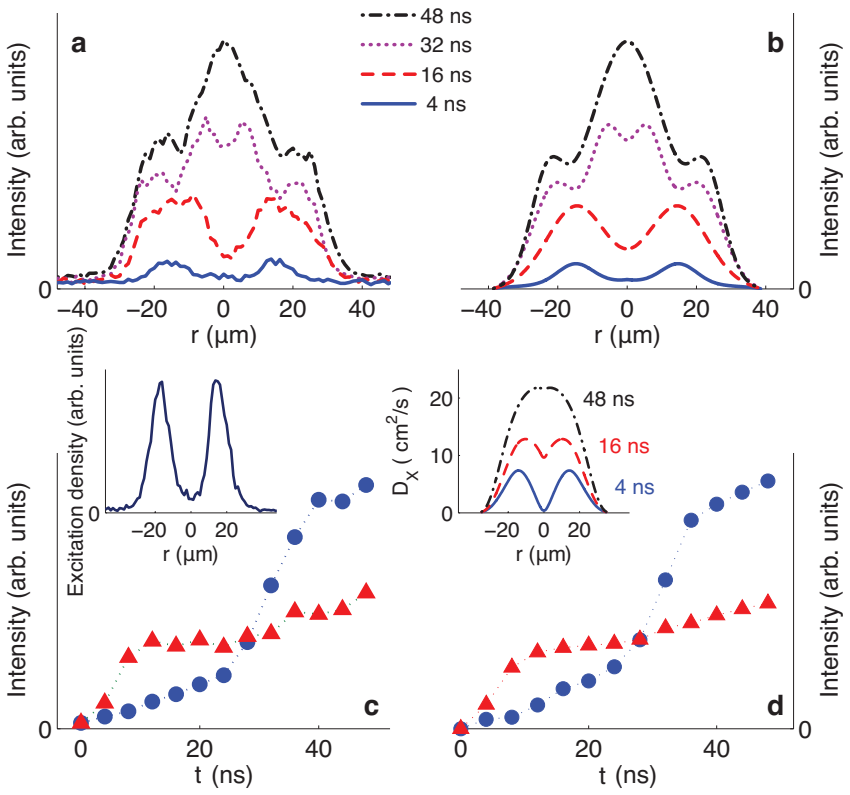

Figure 5.5: Kinetics of the indirect exciton PL profile following the onset of the ring-shaped laser excitation pulse. The measured (a) and calculated (b) cross-sections of the indirect exciton PL across the diameter of the laser excitation ring as a function of time. The measured (c) and calculated (d) indirect exciton PL intensity at the ring center (blue circles) and in the area of the laser excitation ring (red triangles) as a function of time. The time-integration window for each profile (a,b) and point (c,d) is 4 ns. $t = 0$ and $t = 500$ ns correspond to the onset and termination of the rectangular laser excitation pulse, respectively. Left inset: The ring-shaped laser excitation profile. Right inset: The calculated radial dependence of the exciton diffusion coefficient for different time delays. Average excitation power $P_{ex} = 75\,\mu$W. Bath temperature $T_b = 1.4$ K. $V_g = 1.2$ V.

tern reaches a stationary state and, therefore, the trap loading is completed within about 40 ns. Thus the trap loading time is about the lifetime of indirect excitons in this CQW sample (see Figure 5.6c). Note that in another CQW sample with a larger separation between the electron and hole layers the lifetime of indirect excitons reaches several microseconds [Winbow et al., 2007], which is much larger than the trap loading time reported here. However, trap loading on a time scale comparable to the lifetime in the trap is already favorable for studies of confined degenerate gases [Lewandowski et al., 2003; Streed et al., 2006].

Furthermore, for the excitation power used in the experiments, the density of excitons at the trap center reaches $n_x \simeq 1.4 \times 10^{10}\,\mathrm{cm}^{-2}$ within 40 ns. As shown below, the exciton gas is cold, essentially at the lattice temperature, within the area $\sim 100\mu\mathrm{m}^2$ around the trap center. Therefore, $\sim 10^4$ cold excitons are loaded to the trap over the course of 40 ns. The corresponding collection rate of cold excitons to the optically-induced exciton trap exceeds 10^{11} excitons/second.

5.2.3 Simulations

In order to model the experimental data we use the coupled drift-diffusion and thermalization equations and techniques outline in subsection 4.1.3 and subsection 4.2.3

The effective n_x-dependent screening of the disorder potential $U_{\mathrm{rand}}(\mathbf{r})$ by dipole-dipole interacting indirect excitons is crucial for the drastic decrease of the time needed to fill up the optically-induced trap with indirect excitons.

By using Equation 4.7, the time τ_{trav} required for an indirect exciton to travel from the boundary of an annular trap of radius R to its center is estimated as

$$\tau^{(1)}_{\mathrm{trav}} = \frac{R^2}{D^{(0)}_x}\, e^{U^{(0)}/k_B T} \quad \text{for } k_B T \gg u_0 n_x\,, \tag{5.1}$$

$$\tau^{(2)}_{\mathrm{trav}} = \frac{R^2}{D^{(0)}_x}\, \frac{k_B T}{u_0 n^{(0)}_x}\, e^{U^{(0)}/(u_0 n^{(0)}_x)} \quad \text{for } k_B T \ll u_0 n_x\,, \tag{5.2}$$

where $n^{(0)}_x$ is the density of photoexcited indirect excitons at the boundary of

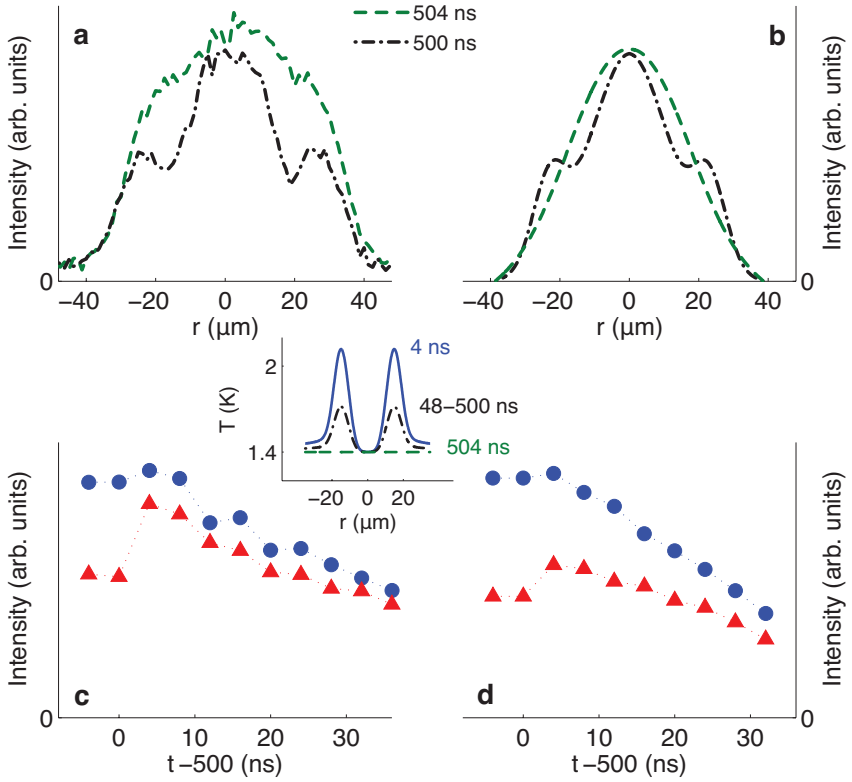

Figure 5.6: Indirect exciton PL following the termination of the ring-shaped laser excitation pulse. The measured (a) and calculated (b) cross-sections of the indirect exciton PL across the diameter of the laser excitation ring as a function of time. The measured (c) and calculated (d) indirect exciton PL intensity at the ring center (blue circles) and in the area of the laser excitation ring (red triangles) as a function of time. The time-integration window for each profile (a,b) and point (c,d) is 4 ns. $t = 0$ and $t = 500$ ns correspond to the onset and termination of the rectangular laser excitation pulse, respectively. Inset: The calculated temperature across the ring diameter in the beginning of the laser excitation pulse at $t = 4$ ns (blue), in the stationary regime achieved during the 500 ns-long excitation pulse about 40 ns after its start $t = 48$ to 500 ns (black), and 4 ns after the termination of the laser excitation pulse at $t = 504$ ns (green). Average excitation power $P_{ex} = 75\,\mu$W. Bath temperature $T_b = 1.4$ K. $V_g = 1.2$ V.

the trap, and the first, low-density limit ($n_x < 10^9\,\mathrm{cm}^{-2}$) refers to the unscreened disorder potential, while the second, high-density limit ($n_x \geq 10^{10}\,\mathrm{cm}^{-2}$) deals with effective mean-field screening of $U_{\mathrm{rand}}(\mathbf{r})$. In the low-density limit, the excitons are essentially localized by disorder, the diffusion coefficient is small, $D_x = D_x^{(0)} \exp[-U^{(0)}/(k_B T)] \sim 0.1\,\mathrm{cm}^2/\mathrm{s}$, and the in-plane transport of excitons out of the excitation spot cannot be seen because in this case $\tau_{\mathrm{trav}}^{(1)} \gg \tau_{\mathrm{opt}}$. In contrast, for $k_B T \ll u_0 n_x$ the diffusion coefficient is large, $D_x = D_x^{(0)} \exp[-U^{(0)}/(u_0 n_x)] \sim 10\,\mathrm{cm}^2/\mathrm{s}$, giving rise to the drastic decrease of the characteristic travel time τ_{trav}: According to Eqs. (5.1)-(5.2), $\tau_{\mathrm{trav}}^{(2)} = \beta \tau_{\mathrm{trav}}^{(1)} \ll \tau_{\mathrm{trav}}^{(1)}$ with the dimensionless smallness parameter $\beta \sim 10^{-3} - 10^{-5}$ (for $T \sim 1\,\mathrm{K}$, $U_0 \sim 1\,\mathrm{meV}$, and $n_x \sim 10^{10}\,\mathrm{cm}^{-2}$). The transition from localized to delocalized indirect excitons is indeed observed with increasing density [Butov et al., 2002; Ivanov et al., 2006; Hammack et al., 2006b].

The calculated change of the exciton diffusion coefficient, due to screening of CQW disorder, is shown in the right inset of Figure 5.5. A drastic increase of D_x with increasing n_x is consistent with the above estimates. For our experiments, evaluations with Equation 5.2 yield $\tau_{\mathrm{trav}}^{(2)} \simeq 4.6\,\mathrm{ns}$ against $\tau_{\mathrm{opt}} \simeq 50\,\mathrm{ns}$, i.e., the condition $\tau_{\mathrm{trav}}^{(2)} \ll \tau_{\mathrm{opt}}$ is clearly met.

The numerical simulations were done by using control parameters consistent with those found in chapter 4. As can be seen in Figure 5.5 and Figure 5.6, the measured and calculated kinetics of the exciton spatial patterns are in quantitative agreement.

When the laser pulse is switched off, a jump in the exciton PL is observed in the region of laser excitation (Figure 5.6). The calculated cooling (i.e. thermalization) time is $\tau_{\mathrm{th}} \simeq 0.2\,\mathrm{ns}$. Both the experiment and calculations show that the exciton cooling time to the lattice temperature is much shorter than the exciton lifetime $\tau_{\mathrm{opt}} \simeq 50$ ns.

More importantly, the data show no PL-jump at the trap center (Figure 5.6). This proves that the excitons at the trap center are cold, essentially at the lattice temperature T_b, even in the presence of the excitation pulse. The numerical simulations of the exciton temperature profile, $T = T(r)$, plotted in the

inset of Figure 5.6 for various time delays, are consistent with this observation. The hierarchy of times, $\tau_{th} \ll \tau_{trav} \ll \tau_{opt}$, results in complete thermalization of indirect excitons during their travel from the boundary of the optically-induced trap to its center, where heating from the laser excitation is negligible.

5.3 Summary

In summary, in this section we proposed and demonstrated a method to trap cold exciton gases with light. This method of optically-induced exciton trapping enables control of a trapping potential *in-situ* by varying the light intensity in space and time. The excitons at the trap center are cold because they are far from the hot laser excitation ring. This method for exciton manipulation has lead to the trapping of a cold gas of excitons in an optically-induced trap and the formation of a highly degenerate Bose gas of excitons in the trap.

Additionally, we have found that the characteristic loading time of an optically-induced trap with cold excitons is on the scale of tens nanoseconds. The observed hierarchy of times (exciton cooling time) < (trap loading time) < (exciton lifetime in the trap) is favorable for the creation of a dense and cold exciton gas in the optically-induced traps and its *in situ* control by varying the excitation profile in space and time before the exciton recombination.

5.4 Acknowledgements

The text of chapter 5, in part, is a reprint of the material as it appears in AT Hammack, M Griswold, LV Butov, LE Smallwood, AL Ivanov, & AC Gossard, *Trapping of cold excitons in quantum well structures with laser light*, Phys Rev Lett **96**, 227402, © 2006 The American Physical Society, where the dissertation author was the first author. The co-authors in this publication directed, supervised, and co-worked on the research with forms the basis of this chapter.

The text of chapter 5, in part, is a reprint of the material as it appears in AT Hammack, LV Butov, L Mouchliadis, AL Ivanov, & AC Gossard, *Kinetics of*

indirect excitons in an optically induced trap in GaAs quantum wells, Phys Rev B **76**, 193308, , where the dissertation author was the first author. The co-authors in this publication directed, supervised, and co-worked on the research with forms the basis of this chapter.

6 Electrical control

In this section we present a method for reducing the dissociative effects of an in-plane electric field on indirect excitons, along with designs for various possible electrostatic exciton traps and an experimental proof of principle for exciton manipulation [Hammack et al., 2006a] and a brief overview of recent developments using electrostatic exciton manipulation. A explanation of the CQWs and diagram of the layer structure for typical structures used for electrostatic manipulation of excitons is presented in section 3.2.

6.1 Proof of principle for electrical control

A possibility of exciton confinement and manipulation in potential traps attracted considerable interest in the past. Excitons are bosonic particles in semiconductors and studies of the bosons in controlled potential reliefs are of fundamental interest. In particular, confinement of bosonic atoms in traps is crucial for experimental implementation of atomic Bose-Einstein condensates [Cornell & Wieman, 2002; Ketterle, 2002]. Also, controlling the optical properties of semiconductors by manipulating the excitons in microdevices may be used to develop new optoelectronic devices.

An advantage of electrostatic control for excitons is a possibility for creating a variety of in-plane potential reliefs with the required parameters for the excitons and a possibility for manipulating the relief in-situ thus controlling the optical properties both in space and in time. In particular, electrostatically induced transport of excitons [Hagn et al., 1995] and the electrostatically controlled capture and release of the photonic images [Krauß et al., 2004] have been

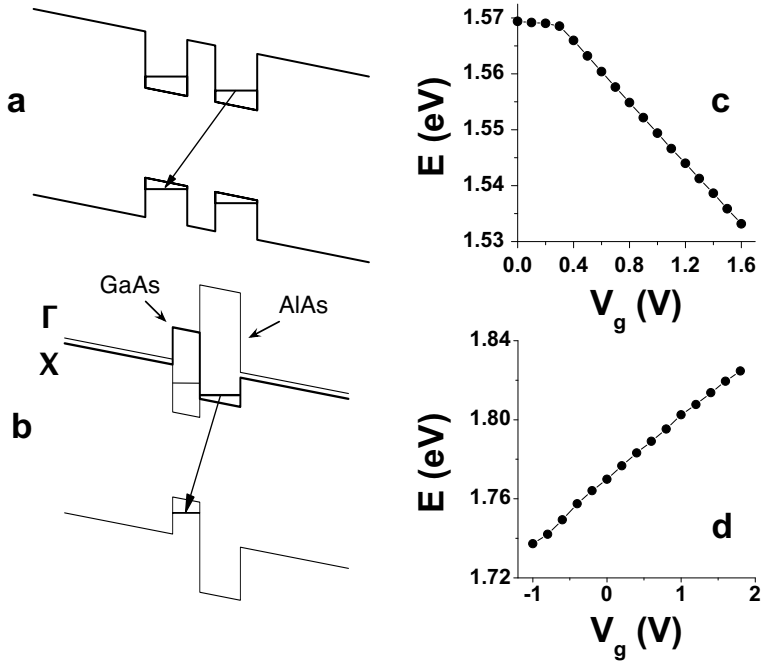

Figure 6.1: Examples of the exciton energy vs gate voltage for GaAs/AlGaAs CQWs (a,c) and AlAs/GaAs CQWs (b,d).

demonstrated.

6.1.1 Model

The principle of the electrostatic traps is based on the quantum confined Stark effect [Miller et al., 1985]: An electric field F_z perpendicular to the QW plane results in the exciton energy shift $\delta E = eF_z d$, where d is the exciton dipole moment. For the indirect excitons in coupled quantum wells (CQWs) [Hagn et al., 1995; Huber et al., 1998] electrons and holes are separated in different QWs and $d \approx L_{QW}$, the distance between the QW centers. The laterally modulated gate voltage $V_g(x, y)$ creates a laterally modulated electric field and, in turn, a lateral relief of the exciton energy $\delta E(x, y) = eF_z(x, y)d$. Control of $V_g(x, y)$ allows manipulation of the in-plane potential profile for excitons both in space and in

time. However, an intrinsic obstacle for exciton confinement in the electrostatic traps is an in-plane electric field F_r that can lead to exciton dissociation [Miller et al., 1985]. A strong exciton confinement in the electrostatic traps requires a strong lateral modulation of V_g, which, in turn, can lead to a strong F_r and exciton ionization [Zimmermann et al., 1997]. In Zimmermann et al. [1997], the intensity of the exciton PL was decreased with increasing modulation of V_g indicating that exciton ionization worked effectively against the exciton confinement to the electrostatic traps.

We modeled electrostatic trap geometries that are variations on the theme of a CQW in an insulating layer sandwiched between a patterned set of top gate electrodes and a single homogeneous bottom gate electrode. To find the field distribution for given voltages at the gate electrodes, the Poisson equation was solved numerically for a static dielectric constant using the boundary elements method [Beer, 2001].

The first trap is studied for AlAs/GaAs CQWs. It is obtained by making a circular hole in the top gate (Figure 6.2). The separation between the gates is taken to be 1000 nm and the exciton dipole moment in AlAs/GaAs CQWs is $d \sim 3.5$ nm. Figure 6.2a displays the calculated effective exciton potential $\delta E(r) = eF_z(r)d$ for a top gate voltage of 1 V for two positions of the CQW — 100 nm and 500 nm above the bottom gate. This trap has only two gates and its spacial profile is controlled by the ratio of the hole diameter versus gate separation. The applied voltage modifies only the strength of the trap (at positive V_g) or bump (at negative V_g), not its shape.

The lateral component of the electric field $F_r(r)$ at the CQW plane is shown in Figure 6.2b. Positioning the CQW close to the lower gate results in a strong suppression of the in-plane electric field at the CQW plane, by an order of magnitude for the example shown in Figure 6.2. This is because the in-plane electric field is concentrated near gate edges and vanishes at the homogeneous bottom gate. The exciton ionization time reduces exponentially with the in-plane electric field $\tau \sim \exp[4E_{ex}/(3eF_r a_{ex})]$, where E_{ex} is the exciton binding energy and a_{ex} is the exciton Bohr radius (see Eqs. A6 and A7 in [Miller

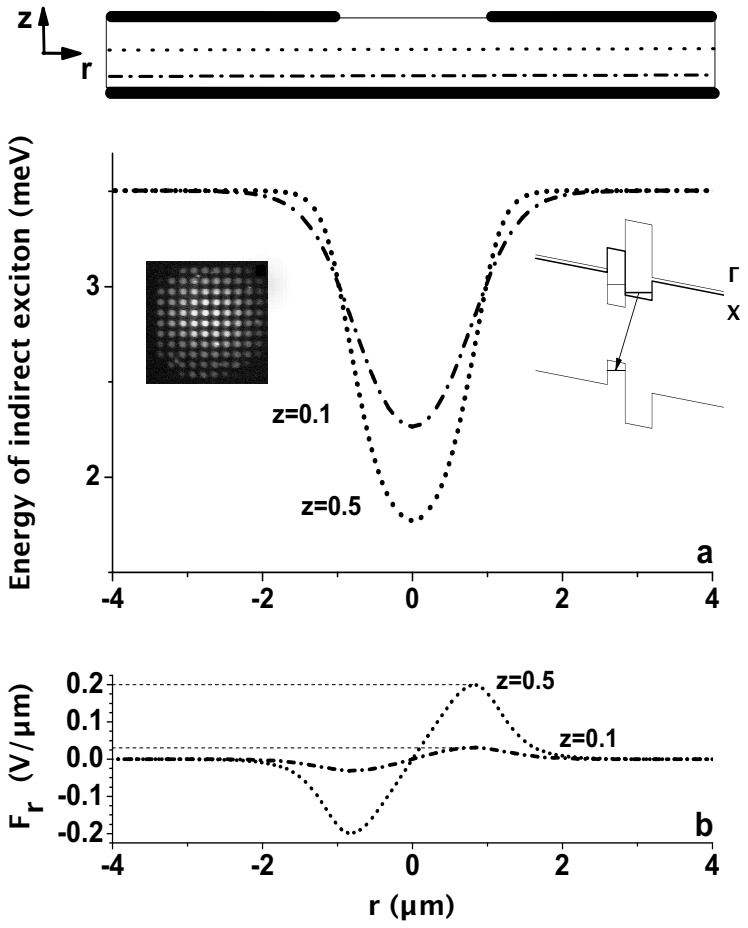

Figure 6.2: Schematic cross-section of an electrostatic trap formed by sandwiching a AlAs/GaAs CQW between a flat bottom gate and a top gate with a hole. The indirect exciton effective potential (a) and lateral component of electric field in the CQW plane (b) are shown for V_g = 1 V, D = 1000 nm, d = 3.5 nm, and for two CQW positions — D_b =100 nm (dotted line, $z = D_b/D$ = 0.1) and 500 nm (dashed line, z = 0.5) above the bottom gate. Inset: the top gate electrode, which forms the periodic trap or bump arrays measured in the experiment.

et al., 1985] for 2D and 3D excitons). If the CQW is equidistant between the gates, the lateral electric fields reach 0.2 V/μm (Figure 6.2b) and the estimated exciton ionization time (using Eq. A6 in [Miller et al., 1985]) is in the ps range and exciton ionization should be prominent. On the other hand, positioning the CQW at the 1/10 distance between the gates, closer to the homogeneous bottom gate, strongly increases the exciton ionization time (by 27 orders of magnitude according to the estimate using Eq. A6 in [Miller et al., 1985]) thus making exciton ionization negligible. At the same time F_z is reduced only weakly and the exciton confinement potential remains strong (Figure 6.2a).

This design can be employed for creation of trap arrays or bump arrays with the modulation amplitude of the potential energy controlled by a single top gate with a periodic array of holes (Figure 6.2). Note that the periodic trap array for excitons, where the modulation amplitude of the potential energy is controlled by a single top electrode, is similar to the optical lattice for atoms, where the modulation amplitude of the potential energy is controlled by the laser intensity [Greiner et al., 2002]. The trap or bump arrays for excitons can be employed to study excitons in externally controlled potentials. Particularly interesting is the possibility to investigate the transition from delocalized to localized excitons (superfluid-insulator transition in the condensate case) with increasing amplitude of the potential, exciton temperature, or density.

The second type of trap is a multi-gated GaAs/AlGaAs CQW structure that allows elaborate control of the radial exciton potential profile (Figure 6.3a). The top gates comprise a system of ten 200 nm wide concentric rings with a ring width vs inter-ring separation ratio of 2:7. The openings between the gates allow exciton photoexcitation over entire trap area while the opening at the trap center allows optical signal collection for the exciton confined at the trap bottom (this is essential when nontransparent gates are used). An important example of potential trap profiles possible for this geometry is a conical trap for the indirect excitons created by linearly increasing gate voltages toward the center of the structure (Figure 6.3a). The trap enables collection of a large number of excitons photoexcited over the entire large trap area at the trap bottom. The large exciton

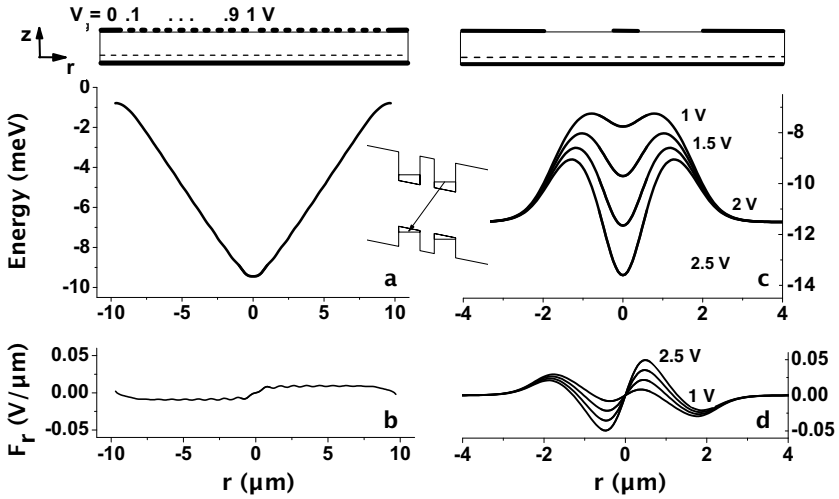

Figure 6.3: The effective potentials and lateral electric fields for a conical trap formed by ten concentric ring electrodes with radially decreasing gate voltages $V_g = 1 - 0$ V (a,b). A trap for evaporative cooling of excitons for $V_g = 1$ V at external gate and $V_{gc} = 1, 1.5, 2, 2.5$ V at center gate (c,d). GaAs/AlGaAs CQW with $D = 1000$ nm, $z = 0.1$, and $d = 12$ nm.

number at the trap bottom is essential for studies of exciton BEC in traps since the critical temperature for BEC increases with the exciton density (for review of exciton condensation in confined systems see e.g. [Butov et al., 2004]). The gradual reduction of the gate voltage distributed over many gate electrodes allows keeping the in-plane electric field negligibly small (Figure 6.3b), thus suppressing the exciton ionization.

The third trap type is designed for evaporative cooling of excitons. It has three gates: a bottom gate, an external top gate, and the central top gate (Figure 6.3c). For central gate voltages $V_{gc} < 1$ V the potential profile is a potential bump for the excitons. However, with the increase of V_{gc} a trap develops at the center of the bump that can be used for evaporative cooling of the indirect excitons: the most energetic excitons overpass the potential barrier and leave the trap thus lowering the temperature of the exciton system in the trap. Evaporative cooling is effectively used for cooling atomic gases in traps [Cornell & Wieman, 2002; Ketterle, 2002].

6.1.2 Experimental proof of principle

Following the computational modeling of the electrostatic exciton traps we fabricated samples based on the first design type (Figure 6.2). The studied electric field tunable $n - i$ AlAs/GaAs CQW structure was grown by MBE. The bottom n^+ layer is Si-doped GaAs with $N_{Si} = 2 \times 10^{18}$ cm^{-2}. It serves as a homogeneous bottom gate. Unlike samples studied in chapter 4 and chapter 5, a surface n^+ layer was not grown for this sample to allow patterning the top gate by evaporated gold contacts. The i-region consists of a 2.5 nm GaAs layer and a 4 nm AlAs layer surrounded by two $Al_{0.48}Ga_{0.52}As$ barrier layers with thicknesses of 900 nm and 100 nm for the upper and lower barriers. Mesas were etched and a patterned top metal electrode containing an array of circular holes with diameters 10 μm and periods 20 μm was deposited onto the mesas. A broad 200 μm open area in the top electrode was fabricated as well for comparison. A schematic of a typical sample structure is shown in figure Figure 6.1. The sample was excited by cw 532 nm laser and the PL signal was diffracted by a single-

grating monochromator then detected using a Peltier cooled photomultiplier tube.

First we note that essentially no change of the exciton energy in the open area vs gate voltage was detected. This indicates that consistent with our calculations an electric field is present in the CQW only in regions close to the upper gate.

The results for the indirect exciton PL for the array of 10 μm holes as a function of gate voltage and excitation power are presented in Figure 6.4. For the CQW type and contact geometry studied, positive applied top gate voltages should cause formation of potential traps beneath the holes in the gate (Figure 6.4a), while negative applied voltages should lead to potential bumps beneath the holes (Figure 6.4b). Figure 6.4c shows that increasing the exciton density leads to enhancement of the PL energy in the trap regime and its reduction in the bump regime. This corresponds to the expected behavior: The indirect excitons are oriented dipoles and interaction between them is repulsive [Butov et al., 2004]. The repulsive interaction leads to enhancement of the exciton energy in the area where the excitons accumulate and, in turn, to reduction of the exciton energy in between the areas of exciton accumulation [Ivanov, 2002] — the repulsively interacting excitons screen the external potential. In the trap regime, the excitons accumulate in the potential traps beneath the holes in the top gate (Figure 6.4a) and the increasing exciton density in the traps is observed in the PL energy enhancement (Figure 6.4c). In contrast, in the bump regime, the excitons accumulate beneath the areas covered by the gates (Figure 6.4b) and the increasing exciton density outside the holes in the top gate is observed in the PL energy reduction (Figure 6.4c). The exciton accumulation in the traps beneath the holes in the top gate is revealed also by the stronger intensity enhancement in the trap regime compared to that in the bump regime (Figure 6.4e).

The transition from the enhancement of the PL energy with density to its reduction is observed around V_g = 0 V (Figure 6.4d). This is expected since the transition from the trap regime to the bump regime takes place at V_g = 0 V for the AlAs/GaAs CQWs. Finally, the formation of the electrostatic exciton

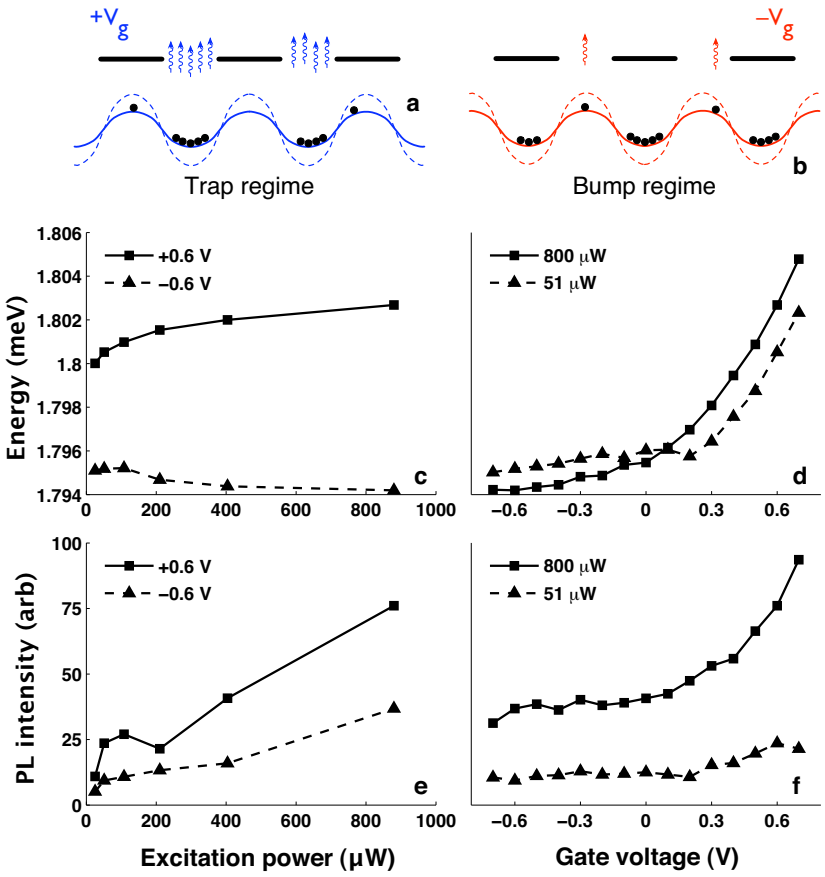

Figure 6.4: Experimental proof of principle for electrostatic trapping of excitons. Top panel: scheme of the expected potential profles for positive V_g, the trap regime (a), and negative V_g, the bump regime (b). The dependence of the PL line energy and intensity on laser excitation power at V_g = 0.6 and -0.6 V (c,e). The dependence of the PL line energy and intensity on gate voltage for two excitation powers (d,f).

traps by the laterally modulated gate voltage at positive V_g is accompanied by enhancement of the exciton PL energy and intensity (Figure 6.4d, f) that is typical for the exciton accumulation in the traps. The observed enhancement of the exciton PL intensity and energy with the electrostatic trap formation shows that the exciton ionization due to the in-plane electric field is suppressed and the excitons accumulate in the traps.

6.2 Excitonic devices

This pioneering work to reduce the dissociation of exciton gases during electrostatic manipulation, has lead to a number devices to control indirect excitons. A brief overview of the work done by my colleagues building upon this foundation is presented in this section.

6.2.1 Exciton confinement

In addition to the proof of principle traps demonstrated earlier during the chapter, we have realized a number of different device architectures to probe the properties of exciton gases. So far we have created elevated traps with increased cooling efficiency [High et al., 2009b,a], a diamond shaped trap and elevated diamond trap (see Figure 6.5), that enable exciton collection over a large spatial region [High et al., 2009a], and linear lattices with tunable amplitude [Remeika et al., 2009] (see Figure 6.5).

6.2.2 Excitonic circuits

Following the creation of methods for the control of the exciton potential energy landscape in CQWs, we have been able to create excitonic circuit devices that enable gated modulation of the flow of excitons, leading to the creation of exciton optoelectric transistors (EXOT) and excitonic circuits (EXIC) that can operate at temperatures up to $\sim 100\,\mathrm{K}$ and at speeds greater than 1 GHz [High et al., 2007, 2008; Grosso et al., 2009]. Figure 6.7 shows the experimental demon-

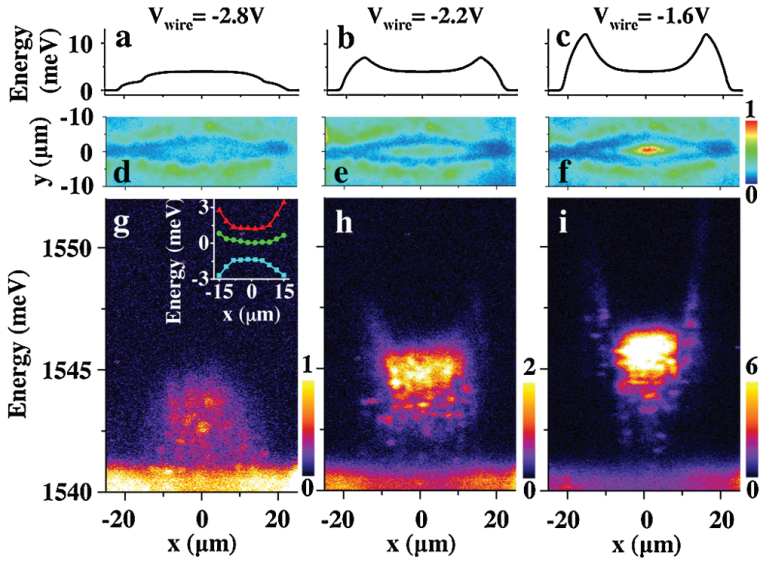

Figure 6.5: (a)(c) Calculated potential profiles vs $|V_{\mathrm{wire}}|$ showing the transition from a bump to elevated trap. The corresponding x-y (d)(f) and x-E (g)(i) emission images of excitons. Inset: the measured trap profile for $|V_{\mathrm{wire}}| = 2.8$ (squares), 2.0 (circles), and 1.6 V (triangles). For all data, $T = 1.4$ K, $\lambda_{\mathrm{ex}} = 633$ nm, $P_{\mathrm{ex}} = 28\,\mu$W, $V_{\mathrm{d}} = 2.5$ V, $V_{\mathrm{p}} = 3$ V. From [High et al., 2009a].

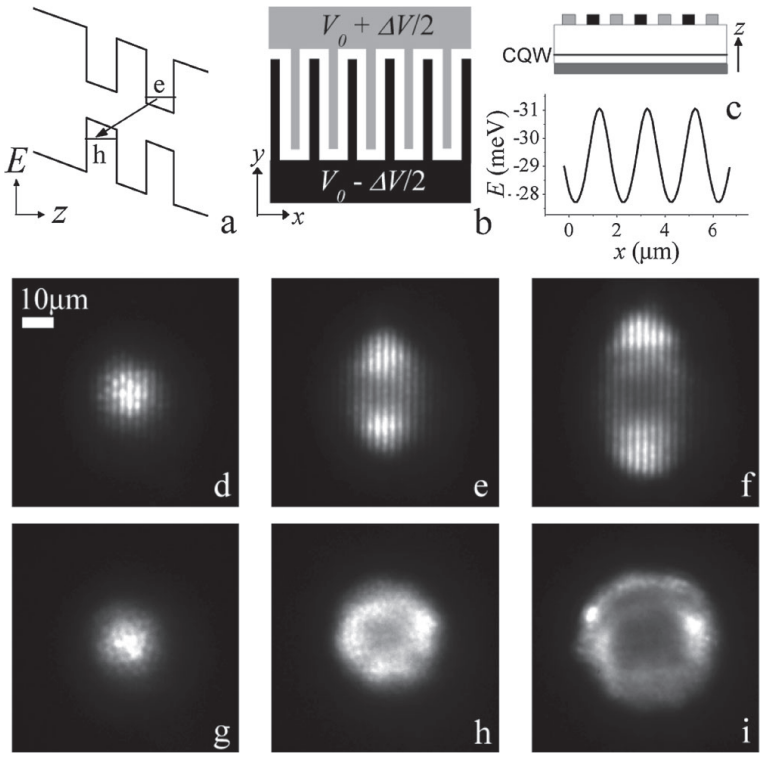

Figure 6.6: (a) Energy band diagram of the CQW. (b),(c) Schematic electrode pattern. The applied base voltage V_0 realizes the indirect regime while the voltage modulation ΔV controls the lattice amplitude. Calculated lattice potential for indirect excitons for $\Delta V = 1\,\mathrm{V}$ is shown in (c). PL images of indirect excitons for lattice amplitude (g)-(i) $\Delta V = 0$ and (d)-(f) $\Delta V = 1.2\,\mathrm{V}$ for excitation powers (d),(g) $P = 0.2$, (e), (h) 3.7, and (f),(i) 12 μW. $T = 1.6\,\mathrm{K}$, $\lambda_{\mathrm{ex}} = 633\,\mathrm{nm}$, and $V_0 = 3\,\mathrm{V}$ for the data.

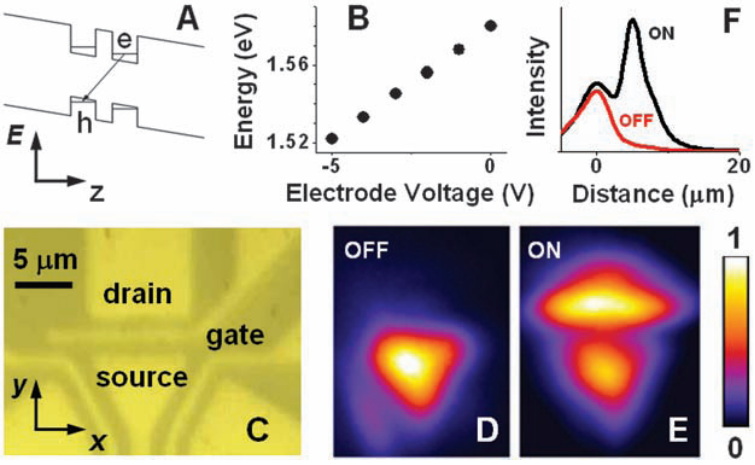

Figure 6.7: Principle and operation of the exciton optoelectronic transistor (EXOT). (A) Energy-band diagram of the CQW structure. e, electron; h, hole. (B) Control of the energy of the indirect excitons by gate voltage. (C to E) Realization of the EXOT. (C) Electrode pattern. [(D) and (E)] Emission of the EXOT in off (D) and on (E) states. The excitons are excited in the source electrode. The energy gradient for the indirect excitons from the source toward the drain is created by the electrode voltages $V_{\text{source}} = -1.5\,\text{V}$ and $V_{\text{drain}} = -2.5\,\text{V}$. The exciton flux is controlled by the gate electrode: $V_{\text{gate}} = 0$ for the off state, and $V_{\text{gate}} = -3\,\text{V}$ for the on state. (F) Emission intensity along the exciton flux for off (red line) and on (black line) regimes [which correspond to the false-color images in (D) and (E)]. From [High et al., 2008].

stration of a functioning exciton transistor that is part of an excitonic circuit. In principle, the operation temperature for excitonic devices can reach room temperature by careful selection of the CQW material and tuning of the QW architecture.

6.3 Summary

In conclusion, we have proposed a design to suppress the in-plane electric field and at the same time to effectively manipulate the potential profile for excitons in the electrostatic traps. This is achieved by positioning the QW plane closer to the laterally homogeneous gate, for instance at the 1/10 distance between the homogeneous bottom gate and patterned top gate. Then, we presented calculations for various types of the electrostatic traps: simple traps for building arrays of wells or bumps, traps for storage of a large exciton number, and traps allowing evaporative cooling for excitons. Finally, we presented experimental proof of principle for trapping of indirect excitons in electrostatic traps.

This research avenue has opened up an extremely exciting field and has already lead to the creation of traps and lattices as well as exitonic circuits.

6.4 Acknowledgements

The text of chapter 6, in part, is a reprint of the material as it appears in AT Hammack, NA Gippius, Sen Yang, GO Andreev, LV Butov, M Hanson, & AC Gossard, *Excitons in electrostatic traps*, J Appl Phys **99**, 066104, © 2006 The American Physical Society, where the dissertation author was the first author. The co-authors in this publication directed, supervised, and co-worked on the research with forms the basis of this chapter.

7 Summary

7.1 Summary

A comprehensive understanding of the exciton transport, generation, recombination, and thermalization processes has lead to the possibility for many exciting techniques to manipulate excitons within the system to form arbitrary region of cold and dense exciton gases. A general purpose model for the evolution of exciton gases combined with various experimental techniques for manipulation comprises the core of the dissertation along with the presentation of numerous methods for exciton control.

To determine the character of exciton transport, generation, recombination, and thermalization we studied steady state and kinetic character of the inner ring in the exciton emission pattern, a feature whose character is determined by the outward flow of excitons from a central excitation spot. The formation time of the inner ring following the onset of the laser excitation is found to be about 30 ns. The inner ring was also found to disappear within 4 ns after the laser termination. The latter process is accompanied by a jump in the PL intensity. The spatial dependence of the PL-jump indicates that the excitons outside of the region of laser excitation, including the inner ring region, are efficiently cooled to the lattice temperature even during the laser excitation. The ring formation and disappearance are explained in terms of exciton transport and cooling and our model matches quantitatively to experimental measurements of the system.

We also proposed and demonstrated a method for optical manipulation of cold exciton gases. Optically-induced exciton manipulation enables control of a laterally modulated potential *in-situ* by varying the light intensity in space and

time. For the excitation ring geometry investigated, the excitons at the ring center are cold because they are far from the hot laser excitation ring. This method for exciton control has lead to the trapping of a cold gas of excitons in an optically-induced trap and the formation of a highly degenerate Bose gas of excitons in the trap. Additionally, we found that loading of excitons to the optically-induced trap occurs on the time scale of tens nanoseconds. The observed hierarchy of times (exciton cooling time) < (trap loading time) < (exciton lifetime in the trap) is favorable for the creation of a dense and cold exciton gas in the optically-induced traps and its *in situ* control by varying the excitation profile in space and time before the exciton recombination.

In conjunction with optical methods for manipulation, we have opened up the field of electrical methods for exciton manipulation, by exploiting the dipole character of indirect excitons. We proposed a design to suppress the in-plane electric field and at the same time to effectively manipulate the potential profile for excitons in the electrostatic traps. Calculations for various types of the electrostatic traps were presented along with experimental proof of principle for the trapping of indirect excitons in electrostatic traps. This research avenue has opened up an extremely exciting field and has already lead to the creation of various exctionic traps and lattices as well as exitonic circuits.

Bibliography

Anderson MH, Ensher JR, Matthews MR, Wieman CE, & Cornell EA. *Observation of Bose-Einstein condensation in a dilute atomic vapor*. Science, **269**(5221), 198 [1995]. doi:10.1126/science.269.5221.198

Ashkin A. *History of optical trapping and manipulation of small-neutral particle, atoms, and molecules*. IEEE Journal Of Selected Topics In Quantum Electronics, **6**(6), 841 [2000]. doi:10.1109/2944.902132

Beer G. *Programming the boundary element method: An introduction for engineers*. Wiley, New York [2001]

Blom PWM, van Hall PJ, Smit C, Cuypers JP, & Wolter JH. *Selective exciton formation in thin GaAs/Al_xGa_{1-x}As quantum wells*. Phys Rev Lett, **71**(23), 3878 [1993]. doi:10.1103/PhysRevLett.71.3878

Bradley CC, Sackett CA, Tollett JJ, & Hulet RG. *Evidence of Bose-Einstein condensation in an atomic gas with attractive interactions*. Phys Rev Lett, **75**(9), 1687 [1995]. doi:10.1103/PhysRevLett.75.1687

Brunner K, Bockelmann U, Abstreiter G, Walther M, Böhm G, Tränkle G, & Weimann G. *Photoluminescence from a single GaAs/AlGaAs quantum dot*. Phys Rev Lett, **69**(22), 3216 [1992]. doi:10.1103/PhysRevLett.69.3216

Butov LV. *Condensation and pattern formation in cold exciton gases in coupled quantum wells*. Journal of Physics: Condensed Matter, **16**(50), R1577 [2004]. doi:10.1088/0953-8984/16/50/R02

Butov LV & Filin AI. *Anomalous transport and luminescence of indirect excitons in AlAs/GaAs coupled quantum wells as evidence for exciton condensation*. Phys Rev B, **58**(4), 1980 [1998]. doi:10.1103/PhysRevB.58.1980

Butov LV, Ivanov AL, Imamoğlu A, Littlewood PB, Shashkin AA, Dolgopolov VT, Campman KL, & Gossard AC. *Stimulated scattering of indirect excitons in coupled quantum wells: Signature of a degenerate Bose-gas of excitons*. Phys Rev Lett, **86**(24), 5608 [2001]. doi:10.1103/PhysRevLett.86.5608

Butov LV, Kulakovskiĭ VD, Lach E, Forchel A, & Grützmacher D. *Magnetoluminescence study of many-body effects in homogeneous quasi-two-dimensional electron-hole plasma in undoped $In_xGa_{1-x}As/InP$ single quantum wells*. Phys Rev B, **44**(19), 10680 [1991]. doi:10.1103/PhysRevB.44.10680

Butov LV, Lai CW, Ivanov AL, Gossard AC, & Chemla DS. *Towards Bose-Einstein condensation of excitons in potential traps*. Nature, **417**, 47 [2002]. doi:10.1038/417047a

Butov LV, Levitov LS, Mintsev AV, Simons BD, Gossard AC, & Chemla DS. *Formation mechanism and low-temperature instability of exciton rings*. Phys Rev Lett, **92**(11), 117404 [2004]. doi:10.1103/PhysRevLett.92.117404

Butov LV, Zrenner A, Abstreiter G, Böhm G, & Weimann G. *Condensation of indirect excitons in coupled AlAs/GaAs quantum wells*. Phys Rev Lett, **73**(2), 304 [1994]. doi:10.1103/PhysRevLett.73.304

Christianen PCM, Piazza F, Lok JGS, Maan JC, & van der Vleuten W. *Magnetic trap for excitons*. Physica B: Condensed Matter, **249-251**, 624 [1998]. doi:10.1016/S0921-4526(98)00273-7

Chu S. *Nobel lecture: The manipulation of neutral particles*. Reviews of Modern Physics, **70**(3), 685 [1998]. doi:10.1103/RevModPhys.70.685

Cohen-Tannoudji CN. *Nobel lecture: Manipulating atoms with photons*. Reviews of Modern Physics, **70**(3), 707 [1998]. doi:10.1103/RevModPhys.70.707

Cornell EA & Wieman CE. *Nobel lecture: Bose-Einstein condensation in a dilute gas, the first 70 years and some recent experiments*. Reviews of Modern Physics, **74**(3), 875 [2002]. doi:10.1103/RevModPhys.74.875

Damen TC, Shah J, Oberli DY, Chemla DS, Cunningham JE, & Kuo JM. *Dynamics of exciton formation and relaxation in GaAs quantum wells*. Phys Rev B, **42**(12), 7434 [1990]. doi:10.1103/PhysRevB.42.7434

Davis KB, Mewes MO, Andrews MR, van Druten NJ, Durfee DS, Kum DM, & Ketterle W. *Bose-Einstein condensation in a gas of sodium atoms*. Phys Rev Lett, **75**(22), 3969 [1995]. doi:10.1103/PhysRevLett.75.3969

Dignam MM & Sipe JE. *Exciton states in coupled double quantum wells in a static electric field*. Phys Rev B, **43**(5), 4084 [1991]. doi:10.1103/PhysRevB.43.4084

Fogler MM, Yang S, Hammack AT, Butov LV, & Gossard AC. *Effect of spatial resolution on the estimates of the coherence length of excitons in quantum wells*. Phys Rev B, **78**(3), 035411 [2008]. doi:10.1103/PhysRevB.78.035411

Fortin E, Fafard S, & Mysyrowicz A. *Exciton transport in Cu_2O: Evidence for excitonic superfluidity?* Phys Rev Lett, **70**(25), 3951 [1993]. doi: 10.1103/PhysRevLett.70.3951

Frenkel J. *On the transformation of light into heat in solids. I.* Physical Review, **37**(1), 17 [1931]. doi:10.1103/PhysRev.37.17

Fukuzawa T, Kano SS, Gustafson TK, & Ogawa T. *Possibility of coherent light emission from Bose condensed states of SEHPs*. Surface Science, **228**(1-3), 482 [1990]. doi:10.1016/0039-6028(90)90358-F

Gärtner A, Holleitner AW, Kotthaus JP, & Schuh D. *Drift mobility of long-living excitons in coupled GaAs quantum wells*. Applied Physics Letters, **89**(5), 052108 [2006]. doi:10.1063/1.2267263

Gärtner A, Prechtel L, Schuh D, Holleitner AW, & Kotthaus JP. *Micropatterned electrostatic traps for indirect excitons in coupled GaAs quantum wells*. Phys Rev B, **76**(8), 085304 [2007]. doi:10.1103/PhysRevB.76.085304

Goto T, Shen MY, Koyama S, & Yokouchi T. *Bose-Einstein statistics of orthoexcitons generated by two-photon resonant absorption in cuprous oxide*. Phys Rev B, **55**(12), 7609 [1997]. doi:10.1103/PhysRevB.55.7609

Greiner M, Mandel O, Esslinger T, Hänsch TW, & Bloch I. *Quantum phase transition from a superfluid to a Mott insulator in a gas of ultracold atoms*. Nature, **415**, 39 [2002]. doi:10.1038/415039a

Grosso G, Graves JC, Hammack AT, High AA, Butov LV, Hanson M, & Gossard AC. *Excitonic switches operating at around 100 K*. Nat Photonics, **3**(10), 577 [2009]. doi:doi:10.1038/nphoton.2009.166

Gulia M, Rossi F, Molinari E, Selbmann PE, & Jugli P. *Phonon-assisted exciton formation and relaxation in $GaAs/Al_xGa_{1-x}As$ quantum wells*. Phys Rev B, **55**(24), R16049 [1997]. doi:10.1103/PhysRevB.55.R16049

Hagn M, Zrenner A, Böhm G, & Weimann G. *Electric-field-induced exciton transport in coupled quantum well structures*. Applied Physics Letters, **67**(2), 232 [1995]. doi:10.1063/1.114677

Hammack AT, Butov LV, Wilkes J, Mouchliadis L, Muljarov EA, Ivanov AL, & Gossard AC. *Kinetics of the inner ring in the exciton emission pattern in coupled GaAs quantum wells*. Phys Rev B, **80**(15), 155331 [2009]. doi: 10.1103/PhysRevB.80.155331

Hammack AT, Gippius NA, Yang S, Andreev GO, Butov LV, Hanson M, & Gossard AC. *Excitons in electrostatic traps*. J Appl Phys, **99**(6), 066104 [2006a]. doi:10.1063/1.2181276

Hammack AT, Griswold M, Butov LV, Smallwood LE, Ivanov AL, & Gossard AC. *Trapping of cold excitons in quantum well structures with laser light*. Phys Rev Lett, **96**(22), 227402 [2006b]. doi:10.1103/PhysRevLett.96.227402

Hänsch TW & Schawlow AL. *Cooling of gases by laser radiation*. Optics Communications, **13**(1), 68 [1975]. doi:10.1016/0030-4018(75)90159-5

Hasuo M, Nagasawa N, Itoh T, & Mysyrowicz A. *Progress in the Bose-Einstein condensation of biexcitons in CuCl*. Phys Rev Lett, **70**(9), 1303 [1993]. doi:10.1103/PhysRevLett.70.1303

High AA, Hammack AT, Butov LV, Hanson M, & Gossard AC. *Exciton optoelectronic transistor*. Opt Lett, **32**(17), 2466 [2007]. doi:10.1364/OL.32.002466

High AA, Hammack AT, Butov LV, Mouchliadis L, Ivanov AL, Hanson M, & Gossard AC. *Indirect excitons in elevated traps*. Nano Lett, **9**(5), 2094 [2009a]. doi:10.1021/nl900605b

High AA, Novitskaya EE, Butov LV, Hanson M, & Gossard AC. *Control of exciton fluxes in an excitonic integrated circuit*. Science, **321**(5886), 229 [2008]. doi:10.1126/science.1157845

High AA, Thomas AK, Grosso G, Remeika M, Hammack AT, Meyertholen AD, Fogler MM, Butov LV, Hanson M, & Gossard AC. *Trapping indirect excitons in a GaAs quantum-well structure with a diamond-shaped electrostatic trap*. Phys Rev Lett, **103**(8), 087403 [2009b]. doi:10.1103/PhysRevLett.103.087403

Huber T, Zrenner A, Wegscheider W, & Bichler M. *Electrostatic Exciton Traps*. Physica Status Solidi (a), **166**(1), R5 [1998]. doi:10.1002/(SICI)1521-396X(199803)166:1<R5::AID-PSSA99995>3.0.CO;2-6

Hulin D, Mysyrowicz A, & Benoît à la Guillaume C. *Evidence for Bose-Einstein statistics in an exciton gas*. Phys Rev Lett, **25**(24), 1970 [1980]. doi:10.1103/PhysRevLett.45.1970

Ivanov AL. *Quantum diffusion of dipole-oriented indirect excitons in coupled quantum wells*. Europhys Lett, **59**(4), 586 [2002]. doi:10.1209/epl/i2002-00144-3

Ivanov AL. *Thermalization and photoluminescence dynamics of indirect excitons at low bath temperatures*. Journal of Physics: Condensed Matter, **16**(35), S3629 [2004]. doi:10.1088/0953-8984/16/35/005

Ivanov AL, Ell C, & Haug H. *Phonon-assisted Boltzmann kinetics of a Bose gas: Generic solution for $T \leq T_c$*. Physical Review E, **55**(6), 6363 [1997]. doi:10.1103/PhysRevE.55.6363

Ivanov AL, Littlewood PB, & Haug H. *Bose-Einstein statistics in thermalization and photoluminescence of quantum-well excitons*. Phys Rev B, **59**(7), 5032 [1999]. doi:10.1103/PhysRevB.59.5032

Ivanov AL, Smallwood LE, Hammack AT, Yang S, Butov LV, & Gossard AC. *Origin of the inner ring in photoluminescence patterns of quantum well excitons*. Europhys Lett, **73**(6), 920 [2006]. doi:10.1209/epl/i2006-10002-4

Kash K, Worlock JM, Sturge MD, Grabbe P, Harbison JP, Scherer A, & Lin PSD. *Strain-induced lateral confinement of excitons in GaAs-AlGaAs quantum well microstructures*. Applied Physics Letters, **53**(9), 782 [1988]. doi: doi:10.1063/1.99832

Keldysh LV. *The electron-hole liquid in semiconductors*. Contemporary Physics, **27**(5), 395 [1986]. doi:10.1080/00107518608211022

Keldysh LV & Kozlov AN. *Collective properties of excitons in semiconductors*. JETP, **27**(3), 521 [1968]

Ketterle W. *Nobel lecture: When atoms behave as waves: Bose-Einstein condensation and the atom laser*. Reviews of Modern Physics, **74**(4), 1131 [2002]. doi: 10.1103/RevModPhys.74.1131

Krauss J, Kotthaus JP, Wixforth A, Hanson M, Driscoll DC, Gossard AC, Schuh D, & Bichler M. *Capture and release of photonic images in a quantum well*. Applied Physics Letters, **85**, 5830 [2004]. doi:10.1063/1.1830676

Kukushkin IV, Kulakovskiĭ VD, & Timofeev VB. *Bose gas of spin-oriented excitons in uniaxially deformed germanium*. JETP Letters, **34**(1), 36 [1981]

Larionov AV, Timofeev VB, Hvam J, & Soerensen K. *Interwell excitons in GaAs/AlGaAs double quantum wells and their collective properties*. JETP, **90**(6), 1093 [2000]. doi:10.1134/1.559200

Levitov LS, Simons BD, & Butov L. *Pattern formation as a signature of quantum degeneracy in a cold exciton system*. Phys Rev Lett, **94**(17), 176404 [2005]. doi: 10.1103/PhysRevLett.94.176404

Lewandowski HJ, Harber DM, Whitaker DL, & Cornell EA. *Simplified system for creating a Bose–Einstein condensate*. Journal of Low Temperature Physics, **132**(5-6), 309 [2003]. doi:10.1023/A:1024800600621

Lin JL & Wolfe JP. *Bose-Einstein condensation of paraexcitons in stressed Cu_2O*. Phys Rev Lett, **71**(8), 1222 [1993]. doi:10.1103/PhysRevLett.71.1222

Lozovik YE & Berman OL. *Phase transitions in a system of two coupled quantum wells*. JETP Letters, **64**(8), 573 [1996]. doi:10.1134/1.567264

Lozovik YE, Ovchinnikov IV, Volkov SY, Butov LV, & Chemla DS. *Quasi-two-dimensional excitons in finite magnetic fields*. Phys Rev B, **65**(23), 235304 [2002]. doi:10.1103/PhysRevB.65.235304

Lozovik YE & Yudson VI. *New mechanism for superconductivity: pairing between spatially separated electrons and holes*. JETP, **71**(8), 738 [1976]

Miller DAB, Chemla DS, Damen TC, Gossard AC, Wiegmann W, Wood TH, & Burrus CA. *Electric field dependence of optical absorption near the band gap of quantum-well structures*. Phys Rev B, **32**(2), 1043 [1985]. doi: 10.1103/PhysRevB.32.1043

Mouchliadis L, Lai CW, & Ivanov AL. *Electric current induced anti-traps for indirect excitons*. Superlattice Microst, **41**(5-6), 392 [2007]. doi: 10.1016/j.spmi.2007.03.018

Mysyrowicz A, Benson E, & Fortin E. *Directed beam of excitons produced by stimulated scattering*. Phys Rev Lett, **77**(5), 896 [1996]. doi: 10.1103/PhysRevLett.77.896

O'Hara KE, Gullingsrud JR, & Wolfe JP. *Auger decay of excitons in Cu_2O*. Phys Rev B, **60**(15), 10872 [1999a]. doi:10.1103/PhysRevB.60.10872

O'Hara KE, Súilleabháin LÓ, & Wolfe JP. *Strong nonradiative recombination of excitons in Cu_2O and its impact on Bose-Einstein statistics*. Phys Rev B, **60**(15), 10565 [1999b]. doi:10.1103/PhysRevB.60.10565

O'Hara KE & Wolfe JP. *Relaxation kinetics of excitons in cuprous oxide*. Phys Rev B, **62**(19), 12909 [2000]. doi:10.1103/PhysRevB.62.12909

Phillips WD. *Nobel lecture: Laser cooling and trapping of neutral atoms*. Reviews of Modern Physics, **70**(3), 721 [1998]. doi:10.1103/RevModPhys.70.721

Rapaport R, Chen G, Snoke DW, Simon SH, Pfeiffer LN, West K, Liu Y, & Denev S. *Charge separation of dense two-dimensional electron-hole gases: Mechanism for exciton ring pattern formation*. Phys Rev Lett, **92**(11), 117405 [2004]. doi: 10.1103/PhysRevLett.92.117405

Reinholz H. *Mott effect for an electron–hole plasma in a two-dimensional structure*. Solid state commun, **123**(11), 489 [2002]. doi:10.1016/S0038-1098(02)00423-4

Remeika M, Graves JC, Hammack AT, Meyertholen AD, Fogler MM, Butov LV, Hanson M, & Gossard AC. *Localization-delocalization transition of indirect excitons in lateral electrostatic lattices*. Phys Rev Lett, **102**(18), 186803 [2009]. doi:10.1103/PhysRevLett.102.186803

Schmitt-Rink S, Chemla DS, & Miller DAB. *Linear and nonlinear optical properties of semiconductor quantum wells*. Advances in Physics, **38**(2), 89 [1989]. doi: 10.1080/00018738900101102

Shevchenko SI. *Theory of superconductivity of systems with pairing of spatially separated electrons and holes*. Fizika Nizkikh Temperatur, **2**, 505 [1976]

Snoke DW, Wolfe JP, & Mysyrowicz A. *Quantum saturation of a Bose gas: Excitons in Cu_2O*. Phys Rev Lett, **59**(7), 827 [1987]. doi:10.1103/PhysRevLett.59.827

Snoke DW, Wolfe JP, & Mysyrowicz A. *Evidence for Bose-Einstein condensation of a two-component exciton gas*. Phys Rev Lett, **64**(21), 2534 [1990]. doi: 10.1103/PhysRevLett.64.2543

Stern M, Garmider V, Segre E, Rappaport M, Umansky V, Levinson Y, & Bar-Joseph I. *Photoluminescence ring formation in coupled quantum wells: Excitonic versus ambipolar diffusion*. Phys Rev Lett, **101**(25), 257402 [2008]. doi: 10.1103/PhysRevLett.101.257402

Streed EW, Chikkatur AP, Gustavson TL, Boyd M, Torii Y, Schneble D, Campbell GK, Pritchard DE, & Ketterle W. *Large atom number Bose-Einstein condensate machines*. Review of Scientific Instruments, **77**(2), 023106 [2006]. doi:10.1063/1.2163977

Strobel R, Eccleston R, Kuhl J, & Köhler K. *Measurement of the exciton-formation time and the electron-and hole-tunneling times in a double-quantum-well structure*. Phys Rev B, **43**(15), 12564 [1991]. doi:10.1103/PhysRevB.43.12564

Szczytko J, Kappei L, Berney J, Morier-Genoud F, Portella-Oberli MT, & Deveaud B. *Determination of the exciton formation in quantum wells from time-resolved interband luminescence*. Phys Rev Lett, **93**(13), 137401 [2004]. doi: 10.1103/PhysRevLett.93.137401

Tamor MA & Wolfe JP. *Drift and diffusion of free excitons in Si*. Phys Rev Lett, **44**(25), 1703 [1980]. doi:10.1103/PhysRevLett.44.1703

Tikhodeev SG. *On the Bose-Einstein condensation of particles with finite lifetime – as demonstrated by excitons*. Solid state commun, **72**(11), 1075 [1989]. doi: 10.1016/0038-1098(89)90250-0

Tikhodeev SG. *Bose-Einstein condensation of finite lifetime particles: Excitons as an example.* JETP, **70**, 380 [1990]

Timofeev VB, Kulakovskiĭ VD, & Kukushkin IV. *Spin aligned exciton gas in uniaxially compressed Ge*. Physica B&C, **117-118**, 327 [1983]. doi:10.1016/0378-4363(83)90519-3

Trauernicht DP, Mysyrowicz A, & Wolfe JP. *Strain confinement and thermodynamics of free excitons in a direct-gap semiconductor*. Phys Rev B, **28**(6), 3590 [1983]. doi:10.1103/PhysRevB.28.3590

Trauernicht DP, Wolfe JP, & Mysyrowicz A. *Highly mobile paraexcitons in cuprous oxide*. Phys Rev Lett, **52**(10), 855 [1984]. doi:10.1103/PhysRevLett.52.855

Vögele XP, Schuh D, Wegscheider W, Kotthaus JP, & Holleitner AW. *Density enhanced diffusion of dipolar excitons within a one-dimensional channel*. Phys Rev Lett, **103**(12), 126402 [2009]. doi:10.1103/PhysRevLett.103.126402

Vörös Z, Balili R, Snoke DW, Pfeiffer LN, & West K. *Long-distance diffusion of excitons in double quantum well structures*. Phys Rev Lett, **94**(22), 226401 [2005]. doi:10.1103/PhysRevLett.94.226401

Wannier GH. *The structure of electronic excitation levels in insulating crystals*. Physical Review, **52**(3), 191 [1937]. doi:10.1103/PhysRev.52.191

Warren JT, O'Hara KE, & Wolfe JP. *Two-body decay of thermalized excitons in Cu_2O*. Phys Rev B, **61**(12), 8215 [2000]. doi:10.1103/PhysRevB.61.8215

Winbow AG, Hammack AT, Butov LV, & Gossard AC. *Photon storage with nanosecond switching in coupled quantum well nanostructures*. Nano Lett, **7**(5), 1349 [2007]. doi:10.1021/nl070386c

Wolfe JP, Hansen WL, Haller EE, Markiewicz RS, Kittel C, & Jeffries CD. *Photograph of an electron-hole drop in germanium*. Phys Rev Lett, **34**(20), 1292 [1975]. doi:10.1103/PhysRevLett.34.1292

Yang S, Butov LV, Levitov LS, Simons BD, & Gossard AC. *Exciton front propagation in photoexcited GaAs quantum wells*. Phys Rev B, **81**(11), 115320 [2010]. doi:10.1103/PhysRevB.81.115320

Yang S, Hammack AT, Fogler MM, Butov LV, & Gossard AC. *Coherence length of cold exciton gases in coupled quantum wells*. Phys Rev Lett, **97**(18), 187402 [2006]. doi:10.1103/PhysRevLett.97.187402

Yoshioka D & MacDonald AH. *Double quantum well electron-hole systems in strong magnetic fields*. Journal of The Physical Society of Japan, **59**, 4211 [1990]. doi:10.1143/JPSJ.59.4211

Zhao W, Stenius P, & Imamoğlu A. *Kinetics of condensation in trapped exciton gases*. Phys Rev B, **56**(9), 5306 [1997]. doi:10.1103/PhysRevB.56.5306

Zhu X, Littlewood PB, Hybertsen MS, & Rice TM. *Exciton condensate in semiconductor quantum well structures*. Phys Rev Lett, **74**(9), 1633 [1995]. doi:10.1103/PhysRevLett.74.1633

Zimmermann R. *Probing exciton condensation by speckled emission*. Solid state commun, **134**(1-2), 43 [2005]. doi:10.1016/j.ssc.2004.06.050

Zimmermann S, Govorov AO, Hansen WL, Kotthaus JP, Bichler M, & Wegscheider W. *Lateral superlattices as voltage-controlled traps for excitons*. Phys Rev B, **56**(20), 13414 [1997]. doi:10.1103/PhysRevB.56.13414

Zrenner A, Worlock JM, Florez L, & Harbison J. *Intrinsic bistability in an optically pumped quantum well structure*. Applied Physics Letters, **56**, 1763 [1990]. doi:10.1063/1.103093